Caging ruthenium complexes with non-toxic ligands for photoactivated chemotherapy

Cuello Garibo, J.A.

APPENDIX I: GENERAL PHOTOCHEMISTRY METHODS

AI.1 Irradiation with a Xe lamp

A LOT Xenon 1000 W lamp was used for the irradiation of NMR tubes and preparative scale photoreaction cells. Depending on the experiment, either IR short pass, >400 nm long pass, and/or 450 nm blue light (450FS10-50 from Andover Corporation) filters were mounted on the lamp. Figure AI.1 shows the transmission spectra of the filters.

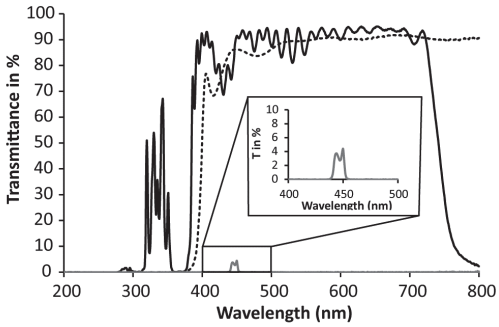

Figure AI.1.Transmittance curves of the IR filter (continuous black), the >400 nm long pass filter (dashes), and the 450 nm band pass filter (grey).

For the photoreactions performed in preparative scale, a 100 mL cylindrical photoreaction cell (d = 5 cm, l = 5 cm) equipped with a water-cooling system was used. Figure AI.2 shows the irradiation setup.

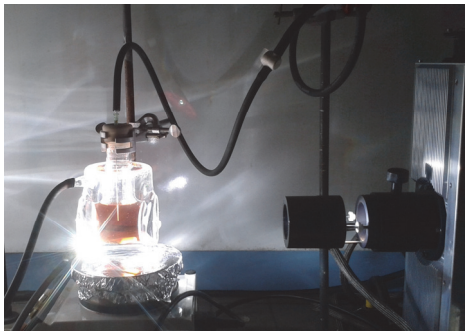

Figure AI.2. Irradiation setup for a preparative scale photoreaction under Ar.

AI.2 Use of Glotaran software for the calculation of the photosubstitution quantum yield.

Upon light irradiation, a complex RuL converts into a complex RuY by photosubstitution of a ligand (L) by a solvent molecule (Y). Considering that both metal complexes are thermally stable, the quantum yield of the photosubstition reaction Φ_{PR} can be calculated by monitoring the photoreaction with UV-vis spectroscopy. As explained in detail by Bahreman and Bonnet,[1] when the irradiation is performed at a wavelength that is not an isosbestic point, the Φ_{PR} can be obtained from the slope of a plot of the number of mol of RuL (n_{RuL}) *vs.* the total number of mol of photons absorbed by RuL from t_0 till t_i (Q_i). Q_i is calculated according to Equation AI.1:

$$Q_i(t) = \sum_{t=0}^{i} q_i$$

Equation AI.1

where q_i is the moles of photons absorbed by RuL between two consecutive UV-vis measurements at t_{i+1} and t_i ($\Delta t = t_{i+1} - t_i$). q_i is calculated according to Equation AI.2:

$$q_i = \left(\frac{(A_{RuL})_{ave}}{(A_e)_{ave}}\right)_i \cdot (1 - 10^{-3\cdot(A_e)_{ave}}) \cdot \varphi \cdot \Delta t$$

Equation AI.2

where $(A_{RuL})_{ave}$ is the average of the absorbance due to RuL between two consecutive UV-vis measurements, $(A_e)_{ave}$ is the average of the absorbance of the solution at the irradiation wavelength between two consecutive UV-vis measurements, $(1 - 10^{-3\cdot(A_e)_{ave}})$ is the probability of absorption of a photon when the irradiation comes from the top and goes through 3 cm pathlength, while all absorbances are measured through a 1 cm pathlength, and φ is the photon flux of the irradiation source at the irradiation wavelength.

The value of $(A_{RuL})_{ave}$, and by extension n_{RuL}, is generally calculated by the two-wavelength method, where the time evolution of the concentrations of the two absorbing species (the reagent and photoproduct) is obtained by following the time evolution of the absorbance at two different wavelengths.[1] However, this method cannot be always used. In some cases the molar extinction coefficient of the photoproduct is unknown, or two sequential photoreactions may take place. In the latter case, the molar extinction coefficients of the intermediate, which cannot be

isolated, is often unknown. In such cases, modelling the evolution of the UV-vis spectra *vs.* time is convenient. In this thesis, we have used Glotaran software for doing this, thus we fitted the time-dependent evolution of the UV-vis spectroscopy data to a kinetic model based on first-order laws, obtaining two output data sets that can be used for the calculation of Φ_{PR}. The first dataset is a collection of globally fitted absorption spectra of the starting complex, the photoproduct, and the intermediate (if any), which makes possible the calculation of the molar extinction coefficient of all the species from that of the starting reagent (Figure AI.3a). The second dataset is the modelled evolution of the relative fractions of the two or three ruthenium species *vs.* irradiation time, here as well according to global fitting (Figure AI.3b). From the time evolution of these fractions and the molar absorption coefficient of all species, the time evolution of n_{RuL} can be calculated, as well as Q_i. The slope of the plot of n_{RuL} *vs.* Q_i (Figure AI.3c) gives the quantum yield of the reaction.

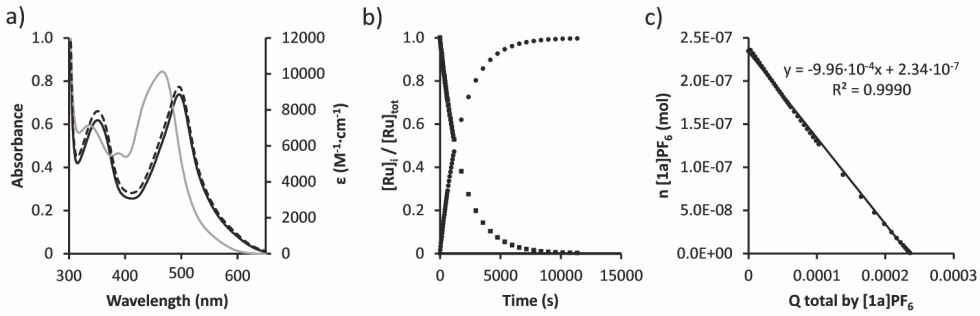

*Figure AI.3. Typical example of Glotaran global fitting of a one-step photochemical reaction, here for the time evolution of the absorbancea of a solution of Λ-[Ru(bpy)$_2$(L-prol)]PF$_6$ (**[1a]**PF$_6$) irradiated in PBS under air, leading to photooxidation (Chapter 2). a) Left axis: globally fitted absorption spectra of **[1a]**PF$_6$ (black) and Λ-[Ru(bpy)$_2$(L-prol − 2H)]PF$_6$ ([7]PF$_6$) (grey). Right axis: experimental spectrum of **[1a]**PF$_6$. b) Modelled evolution of the relative concentrations of **[1a]**PF$_6$ (squares) and [7]PF$_6$ (circles) vs. irradiation time according to global fitting. c) Plot of the amount of **[1a]**PF$_6$ (mol) vs. total amount of photons absorbed by **[1a]**PF$_6$ (mol). The slope of the obtained line is the opposite of the photooxidation quantum yield. Conditions: 0.078 mM solution of **[1a]**PF$_6$ in PBS irradiated at 298 K in air using a 493 nm LED at 1.61·10^{-7} mol·s^{-1}.*

AI.3 Singlet Oxygen quantum yield measurement

The quantum yield of singlet oxygen generation was determined in a custom-built setup (Figure AI.4), in which both UV-vis absorption and infrared emission spectroscopy could be performed. All optical parts were connected with optical fibers from Avantes (Apeldoorn, The Netherlands), with a diameter of 200-600 µm. For each measurement, 500 µL of sample, consisting of the compound in deuterated methanol ($A_{450} \leq 0.1$ for 4.0 mm pathlength), was placed in a stirred 104F-OS semi-micro

fluorescence cuvette (Hellma Analytics, Müllheim, Germany) in a CUV-UV/VIS-TC temperature-controlled cuvette holder from Avantes. The sample was allowed to equilibrate at 293 K for 5 min. Emission spectroscopy was performed with a 450 nm fiber-coupled laser (Laser system LRD-0450; Laserglow, Toronto, Canada), at 50 mW optical power (4 mm beam diameter; 0.4 $W \cdot cm^{-2}$) at a 90° angle with respect to the spectrometer. The excitation power was measured using a S310C thermal sensor connected to a PM100USB power meter (Thorlabs, Dachau, Germany). Infrared emission spectra were measured from 1000 nm to 1400 nm using an Avantes NIR256-1.7TEC spectrometer, The infrared emission spectrum was acquired within 9 s, after which the laser was turned off directly. UV-vis absorption spectra before and after emission spectroscopy were measured using an Avalight-DHc halogen-deuterium lamp (Avantes) as light source (turned off during emission spectroscopy) and an Avantes 2048L StarLine UV-vis spectrometer as detector, both connected to the cuvette holder at a 180° angle. No difference in UV-vis absorption spectrum was found due to exposure to the blue laser, showing that the singlet oxygen emission is that of the starting compound. All spectra were recorded with Avasoft 8.5 software from Avantes and further processed with Microsoft Office Excel 2010 and Origin Pro 9.1 software.

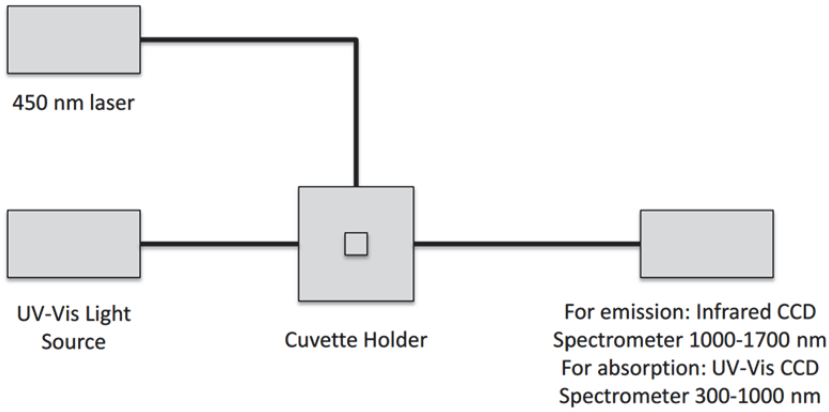

Figure AI.4. Setup for $^1O_2$ quantum yield measurement.

The quantum yield of singlet oxygen production was calculated using the relative method with $[Ru(bpy)_3]Cl_2$ as the standard (Φ_Δ = 0.73 in CD_3OD),[2] according to Equation 7.1:

$$\Phi_{\Delta,sam} = \Phi_{\Delta,std} \times \frac{A_{450,std}}{A_{450,sam}} \times \frac{E_{sam}}{E_{std}}$$

Equation 7.1

where Φ_{Δ} is the quantum yield of singlet oxygen generation, A_{450} is the absorbance at 450 nm, E is the integrated emission peak of singlet oxygen at 1274 nm, and *sam* and *std* denote the sample and standard, respectively.

AI.4 References

1. A. Bahreman, J.-A. Cuello-Garibo and S. Bonnet, *Dalton Trans.*, **2014**, 43, 4494-4505.
2. D. Garcìa-Fresnadillo, Y. Georgiadou, G. Orellana, A. M. Braun and E. Oliveros, *Helv. Chim. Acta*, **1996**, 79, 1222-1238.

APPENDIX II: CELL CULTURE AND (PHOTO)CYTOTOXICITY STUDIES

AII.1 General:

Human cancer cell line A549 (human lung carcinoma) was distributed by the European Collection of Cell Cultures (ECACC), and purchased from Sigma Aldrich. Dulbecco's Modified Eagle Medium (DMEM, with and without phenol red, without glutamine), Glutamine-S (GM;200 mm), trichloroacetic acid (TCA), glacial acetic acid, sulfo-rhodamine B (SRB), and tris(hydroxylmethyl)aminomethane (Trisbase) were purchased from Sigma Aldrich. Fetal calf serum (FCS) was purchased from Hyclone. Penicillin and streptomycin were purchased from Duchefa and were diluted to a 100 mg/mL penicillin/streptomycin solution (P/S). Trypsin and OptiMEM (without phenol red) were purchased from Gibco Life Technologies. Trypan blue (0.4% in 0.81% sodium chloride and 0.06% potassium phosphate dibasic solution) was purchased from BioRad. Plastic disposable flasks and 96-well plates were purchased from Sarstedt. Cells were counted by using a BioRad TC10 automated cell counter with Biorad cell-counting slides. UV-vis measurements for analysis of 96-well plates were performed with a M1000 Tecan Reader. Cells were inspected with an Olympus IX81 microscope.

AII.2 Cell culture

Cells were cultured in Dulbecco's Modified Eagle Medium containing phenol red, supplemented with 8.0% v/v FCS, 0.2% v/v P/S and 0.9% v/v glutamax. Cells were incubated at 37 ºC at 7.0% CO_2 in 75 cm^2 T-flasks and splitted once a week at 80-90% confluency. Cells were cultured for a maxium of 8 weeks for all biological experiment, and passaged at least twice after being thawed.

AII.3 Cell-irradiation setup

The cell-irradiation system consisted of a Ditabis thermostat (980923001) fitted with two flat-bottomed micro-plate thermoblocks (800010600) and a 96-LED array fitted to a standard 96-well plate. The 454 nm LED (OVL-3324), 520 nm LED (OVL-3324), fans (40 mm, 24 VDC, 9714839), and power supply (EA-PS 2042-06B) were obtained from Farnell. See Hopkins *et al.* for a full description.[1]

AII.4 Cytotoxicity assays

A549 cells were seeded at t = 0 in 96-well plates at a density of 5000 cells/well (100 µL) in OptiMEM supplemented with 2.4% v/v FCS, 0.2% v/v P/S, and 1.0% v/v glutamax (called OptiMEM complete) and incubated for 24 h at 37 ºC and 7.0% CO_2. After this period, aliquots (100 µL) of six different concentrations of freshly prepared stock solutions of the compounds in OptiMEM were added to the wells in triplicate (see plate design in Figure AII.1). Sterilized dimethylsulfoxide (DMSO) was used to dissolve the compounds in such amounts that the maximum v/v% of DMSO per well did not exceed 0.5%. For every irradiated plate a parallel control plate was prepared and treated identically, but without irradiation. Plates were incubated in the dark for an additional time. After this period, half of the plates were irradiated and the other half were kept in the dark. After irradiation, all the plates were incubated in the dark until a total time of 96 h after seeding (see the respective Experimental Section for the details). The cells were fixated by adding cold TCA (10 % w/v; 100 µL) in each well and the plates were stored at 4 ºC for at least 4 h as part of the sulforhodamine B (SRB) assay that was adapted from Vichai *et al*.[2] In short, after fixation, TCA medium mixture was removed from the wells, rinsed with demineralized water three times, and air dried. Then, each well was stained with 100 µL SRB (0.6% w/v in 1% v/v acetic acid) for 30 min, the SRB was removed by washing with acetic acid (1 % v/v), and air dried. The SRB dye was solubilized with Tris base (10 mM; 200 µL), and the absorbance in each well was read at λ = 510 nm by using a M1000Tecan Reader.

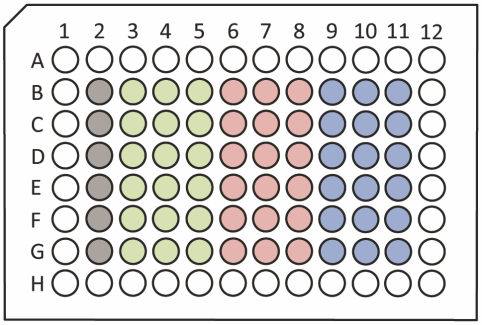

Figure AII.1. Design of a 96-well plate used in the cytotoxicity assays. Grey: non-treated cells (n_t = 6); green:cells treated with compound A with six different concentrations (one per row) per triplicate (n_t = 3); red: cells treated with compound B with six different concentrations (one per row) per triplicate (n_t = 3); blue:cells treated with compound C with six different concentrations (one per row) per triplicate (n_t = 3).

The SRB absorbance data per compound per concentration was averaged over three identical wells (technical replicates, n_t = 3) in Excel and made suitable for use in GraphPad Prism. Relative cell populations were calculated by dividing the average absorbance of the treated wells by the average absorbance of the untreated wells. In any case, it was checked that the cell viability of the untreated cells of the samples irradiated were similar (maximum difference of 10%) to the non-irradiated samples to make sure no harm was done by light alone. The data from three independent biological replications was plotted versus log(concentration in μM). The resulting dose-response curve for each compound under dark and irradiated conditions was fitted to a non-linear regression function with fixed *y* maximum (100%) and minimum (0%) (relative cell viability) and a variable Hill slope, to obtain the effective concentration (EC_{50} in μM). The simplified two-parameter Hill-slope equation used for the fitting is shown in Equation AII.1:

$$\frac{100}{\left(1+10^{\left((\log_{10}EC50-X)\cdot Hill\ slope\right)}\right)}$$

Equation AII.1

Photo indices (PI) reported in Table 3.1, Table 4.3, and Table 6.3 were calculated, for each compound, by dividing the EC_{50} value obtained in the dark by the EC_{50} value determined under light irradiation.

AII.5. References

1. S. L. Hopkins, B. Siewert, S. H. C. Askes, P. Veldhuizen, R. Zwier, M. Heger and S. Bonnet, *Photochem. Photobiol. Sci.*, **2016**, 15, 644-653.
2. V. Vichai and K. Kirtikara, *Nat. Protocols*, **2006**, 1, 1112-1116.

APPENDIX III SUPPORTING INFORMATION FOR CHAPTER 2

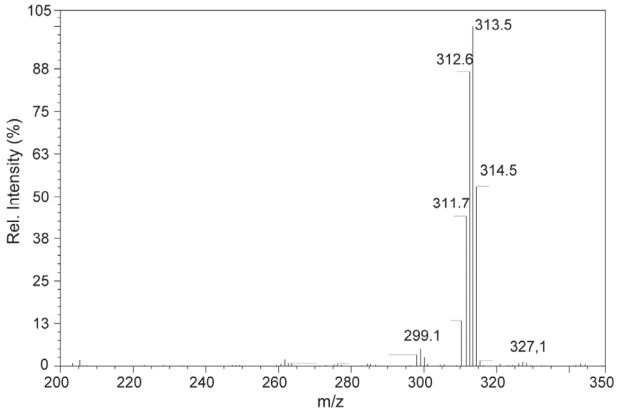

*Figure AIII.1. Mass spectrum of complex [**5**]$^{2+}$ with a calcd m/z = 313.1. [Ru(dmbpy)$_3$]$^{2+}$ and [Ru(bpy)$_2$(dmbpy)]$^{2+}$ resulting from limited ligand scrambling are present with calcd m/z = 327.1 and 299.1, respectively.*

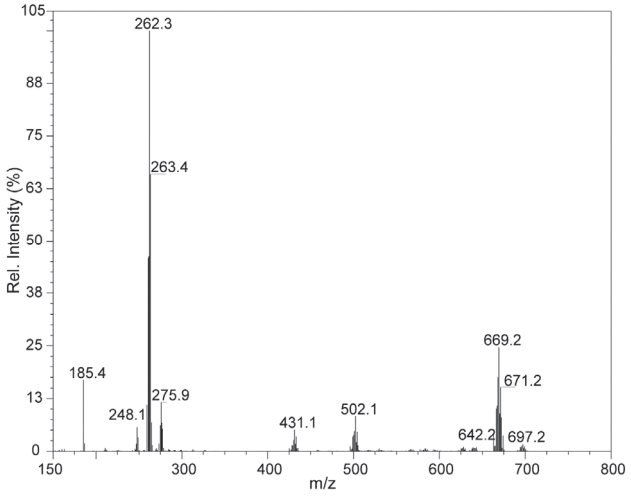

*Figure AIII.2. Mass spectrum after photolysis of a CH$_3$CN solution of [**5**]PF$_6$ under Ar and at 25 °C with peaks corresponding to the free ligand {dmbpy + H}$^+$ (calcd m/z = 185.2), [Ru(bpy)(dmbpy)(CH$_3$CN)$_2$]$^{2+}$ (calcd m/z =262.1), [Ru(bpy)$_2$(CH$_3$CN)$_2$]$^{2+}$ (calcd m/z =248.1), [Ru(dmbpy)$_2$(CH$_3$CN)$_2$]$^{2+}$ (calcd m/z =276.1), {[Ru(bpy)$_2$(CH$_3$CN)$_2$]PF$_6$}$^+$ (calcd m/z =642.1), {[Ru(bpy)(dmbpy)(CH$_3$CN)$_2$]PF$_6$}$^+$ (calcd m/z =669.1), and {[Ru(dmbpy)$_2$(CH$_3$CN)$_2$]PF$_6$}$^+$ (calcd m/z = 697.1).*

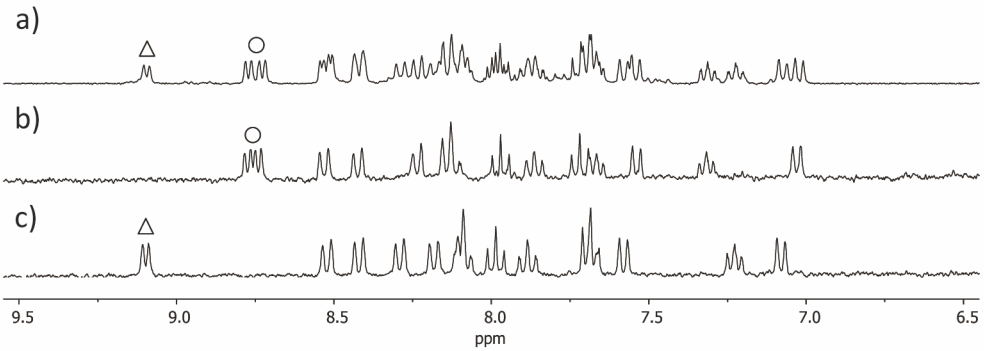

*Figure AIII.3. ^{1}H NMR spectra (region 6.5 – 9.5 ppm) in D_2O of a) the crude reaction mixture containing **[2a]**PF_6 and **[2b]**PF_6; b) fraction A of the chromatography column on alumina containing complex **[2a]**PF_6 (round); and c) fraction B containing complex **[2b]**PF_6 (triangle).*

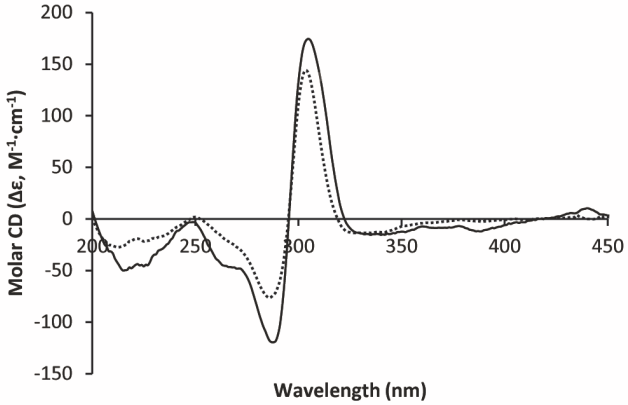

*Figure AIII.4. Circular dichroism spectra of a solution of **[2a]**PF_6 (continuous) and **[2b]**PF_6 (dashed) in water with concentrations of $3.27 \cdot 10^{-5}$ M and $6.50 \cdot 10^{-5}$ M, respectively, in a 0.1 cm path length cuvette.*

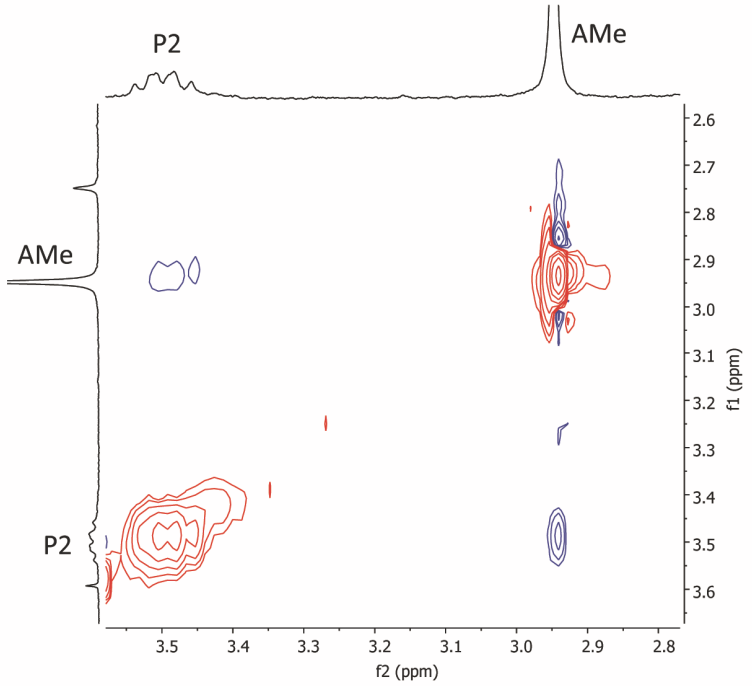

*Figure AIII.5. NOESY NMR spectrum of a solution of **[2a]**PF_6 in D_2O showing an off-diagonal peak between the α proton P2 and the methyl peak AMe of dmbpy.*

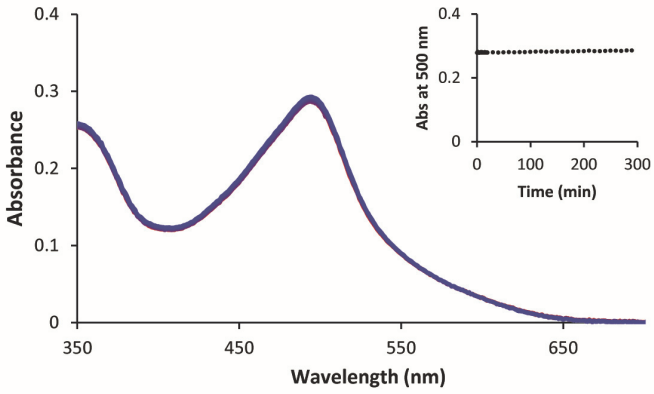

*Figure AIII.6. Evolution of the UV-vis spectra (region 350 – 700 nm) of a solution of **[1a]**PF_6 in PBS (0.035 mM) in the dark at 310 K under air.*

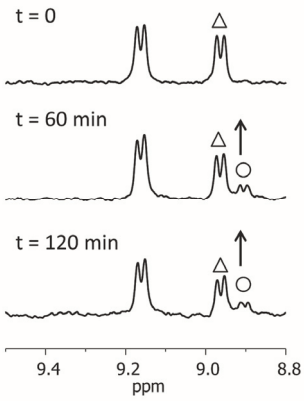

*Figure AIII.7. Evolution of the ^{1}H NMR spectra (region 8.5 – 9.5 ppm) of the irradiation of **[1a]**PF_6 at 310 K in deuterated PBS (pD=7.8) under Ar. The doublet at 9.16 ppm (triangle) corresponds to the H_6 proton on the bpy for complex **[1a]**$^+$ and the arising doublet at 8.90 ppm corresponds to the H_6 proton on the bpy for the delta isomer. Concentration of **[1a]**PF_6 = 0.45 mM.*

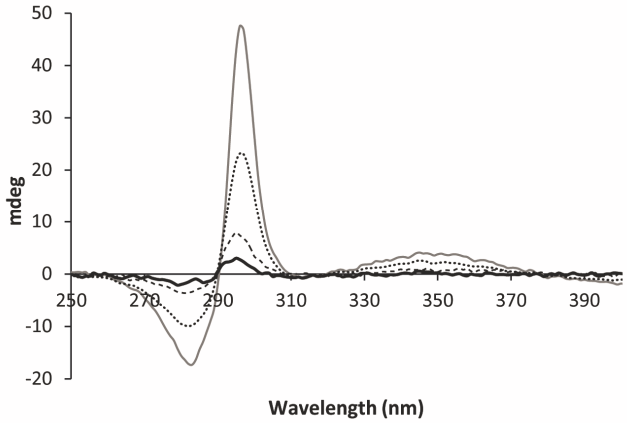

*Figure AIII.8. Circular dichroism spectra (region 250 – 400 nm) of a solution of **[1a]**PF_6 in PBS in a 0.1 cm cuvette before (grey continuous) and after irradiation with a 493 nm LED in the following conditions. Dots: under Ar; dashed: under air with 5 mM GSH; black continuous: under air. Detailed conditions of the photo reactions are given in Table AIII.1.*

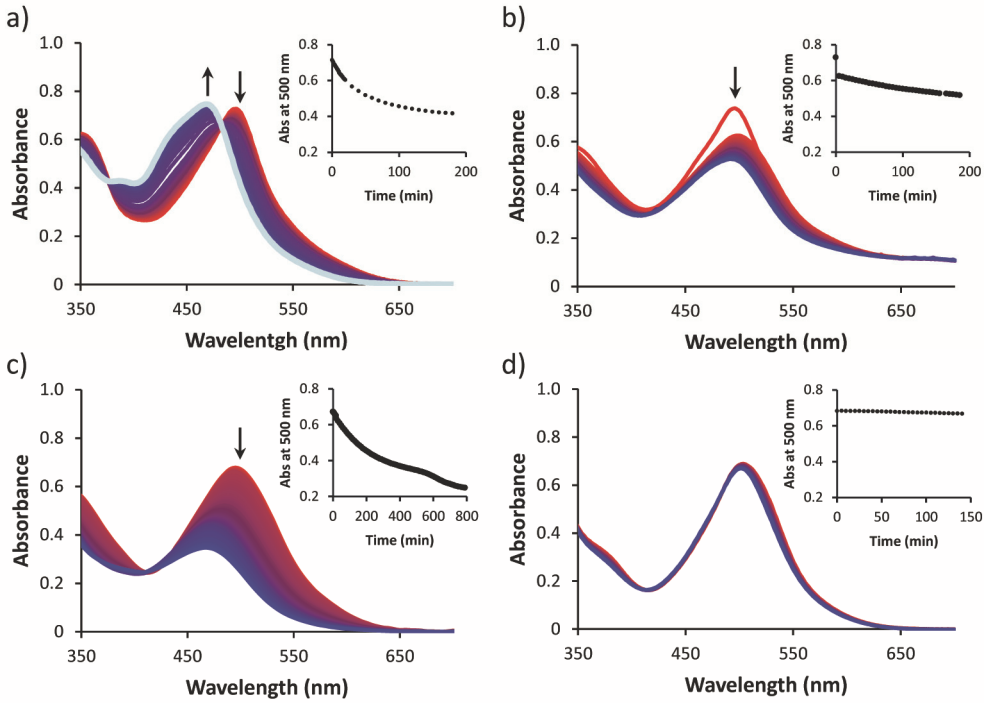

*Figure AIII.9. Evolution of the UV-vis spectra (region 350 – 700 nm) of an irradiated solution of a) [**1a**]PF_6 (0.078 mM) with 5mM of GSH, b) [**2a**]PF_6 (0.032 mM), c) [**2b**]PF_6 (0.087 mM), and d) [**3a**]PF_6 (0.077 mM) in PBS at 298 K under air. Conditions are detailed in Table AIII.1.*

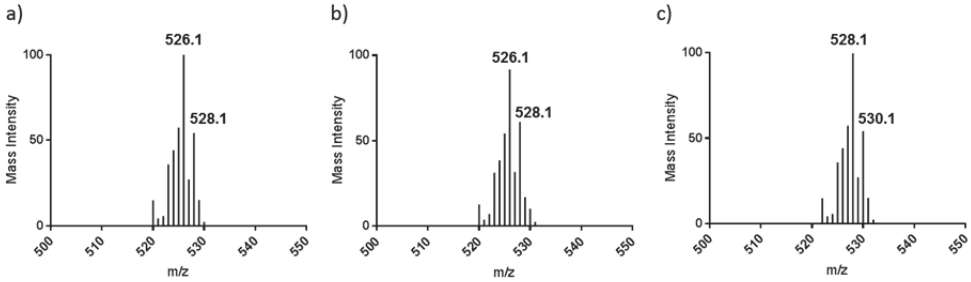

Figure AIII.10. Calculated isotope pattern of a) $[7]^+$, b) a mixture 7:3 of $[1]^+$:$[7]^+$, and c) $[1]^+$.

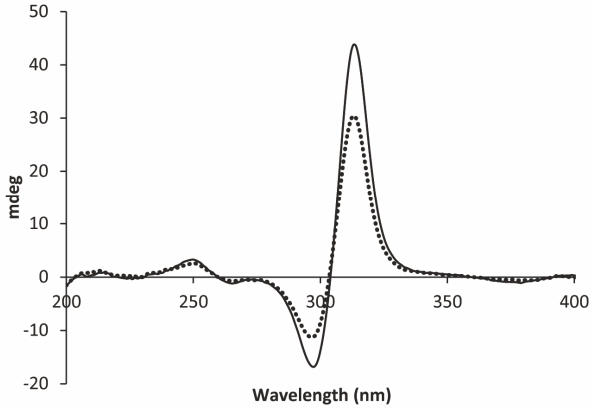

*Figure AIII.11. Circular dichroism spectra (region 200 – 400 nm) of a solution of [**3a**]PF_6 in PBS before (continuous) and after 140 min light irradiation (doted) using a 493 nm LED under air. Conditions are detailed in Table AIII.1.*

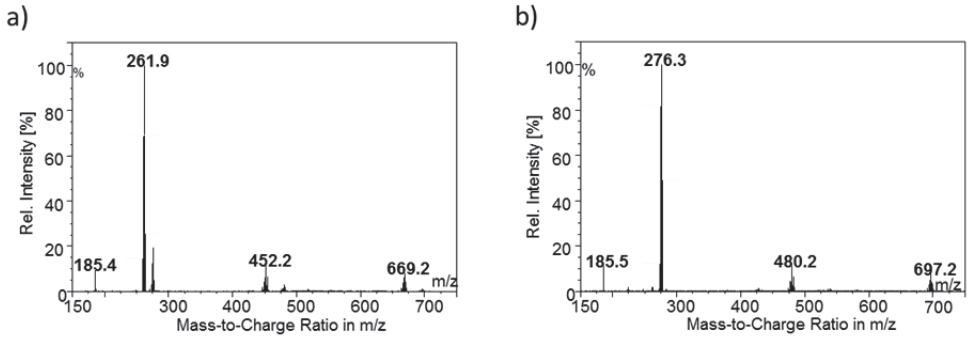

*Figure AIII.12. Mass spectrum of acetonitrile solutions of (a) [**2a**]PF_6 and (b) [**3a**]PF_6 after the irradiation with a 493 LED. a) Peaks corresponding to {dmbpy + H}$^+$ (calcd m/z = 185.2), [Ru(bpy)(dmbpy)$(CH_3CN)_2]^{2+}$ (calcd m/z = 262.1), [Ru(bpy)(L-Prol − 2H)$(CH_3CN)_2]^+$ (calcd m/z = 452.1), and {[Ru(bpy)(dmbpy)$(CH_3CN)_2]PF_6$}$^+$ (calcd m/z = 669.1). b) Peaks corresponding to {dmbpy + H}$^+$ (calcd m/z = 185.2), [Ru(dmbpy)$_2(CH_3CN)_2]^{2+}$ (calcd m/z = 276.1), [Ru(dmbpy)(L-Prol − 2H)$(CH_3CN)_2]^+$ (calcd m/z = 480.1), and [Ru(dmbpy)$_2(CH_3CN)_2]PF_6$}$^+$ (calcd m/z = 697.1). Conditions are detailed in Table AIII.1.*

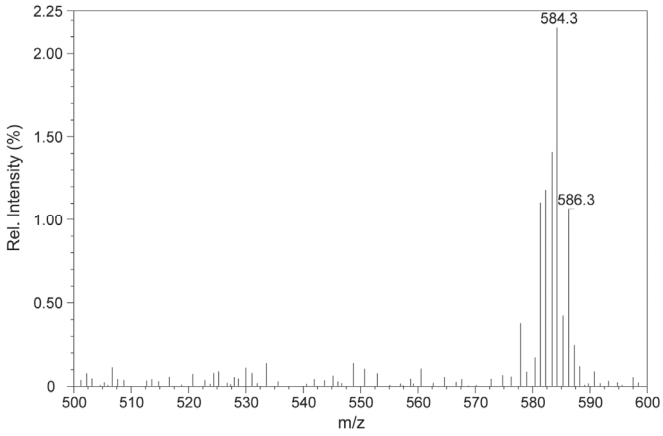

Figure AIII.13. Mass spectrum after 140 min irradiation with a 493 nm LED of a solution of ***[3a]***PF_6 *in PBS (0.077 mM) under air with a peak corresponding to* ***[3a]***$^+$ *(calcd m/z = 584.1). Conditions of the irradiation are detailed in Table AIII.1.*

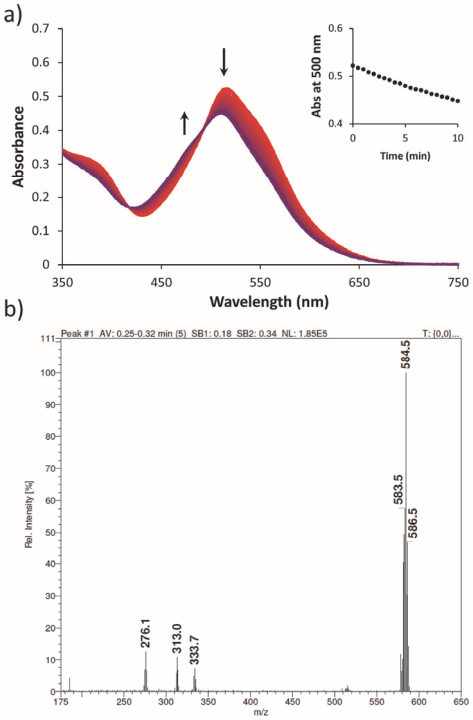

Figure AIII.14. a) Evolution of the UV-vis spectra of a solution of ***[3a]***PF_6 *(0.062 mM) in* CH_3CN *upon irradiation for 10 min under Ar with a 493 nm LED with a photon flux of* $1.61 \cdot 10^{-8}$ *mol·*s^{-1}*. b) Mass spectrum after 10 min irradiation of solution in (a) with peaks corresponding to* $[Ru(dmbpy)_2(CH_3CN)_2]^{2+}$ *(calcd m/z = 276.1),* $[Ru(dmbpy)_2(L\text{-}Hprol)(CH_3CN)]^{2+}$ *(calcd m/z = 313.1),* $[Ru(dmbpy)_2(L\text{-}Hprol)(CH_3CN)_2]^{2+}$ *(calcd m/z = 333.6), and* $[Ru(dmbpy)_2(L\text{-}prol)]^+$ *(calcd m/z = 584.2).*

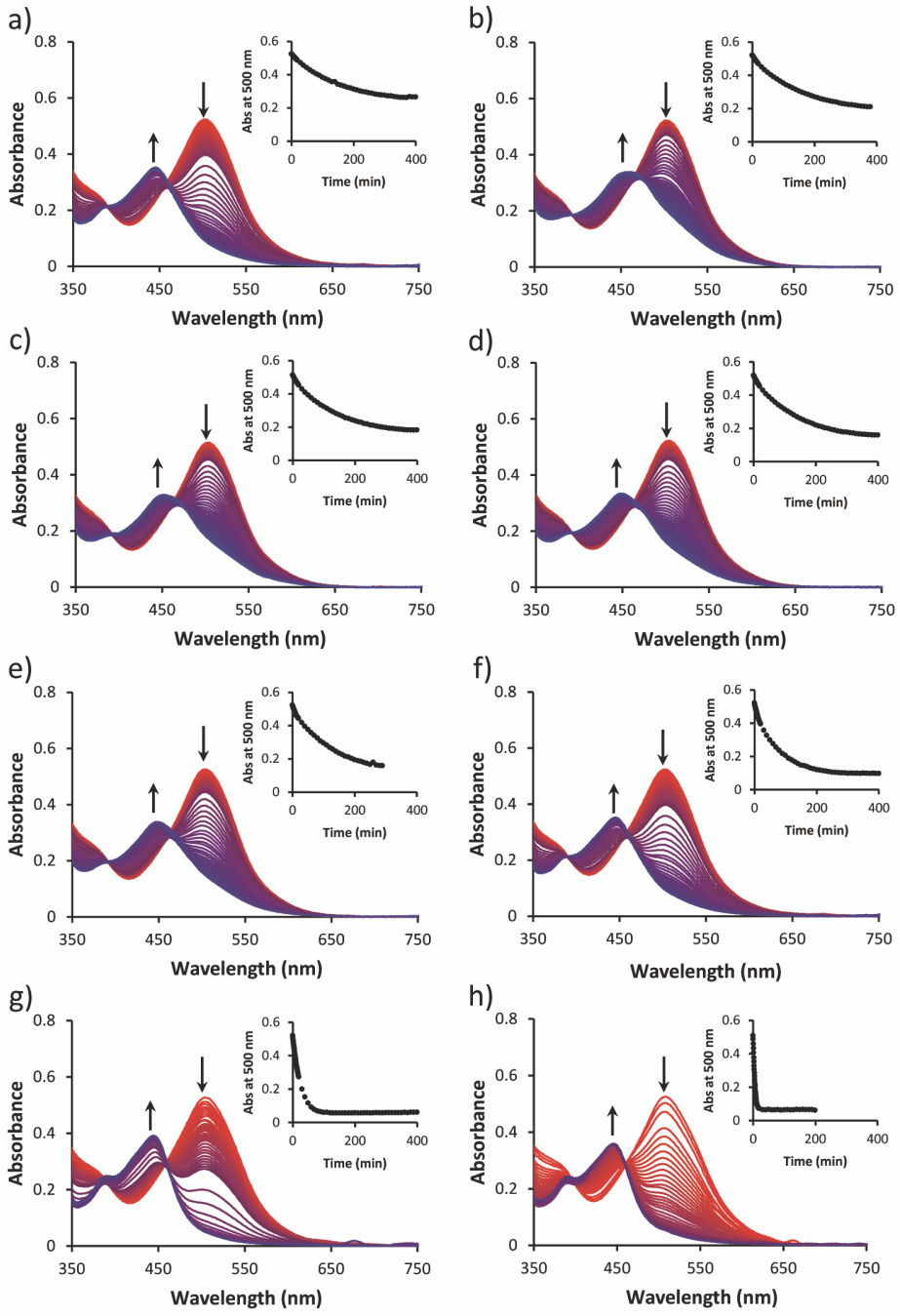

*Figure AIII.15. Evolution of the UV-Vis spectra of a solution of [**3a**]PF_6 (0.062 mM) in water with a) 1% CH_3CN, b) 2% CH_3CN, c) 3% CH_3CN, d) 4% CH_3CN, e) 5% CH_3CN, f) 10% CH_3CN, g) 30% CH_3CN, and h) 80% CH_3CN upon irradiation under Ar with a 493 nm LED with a photon flux of $1.13 \cdot 10^{-7} - 1.16 \cdot 10^{-7}$ mol·s^{-1}.*

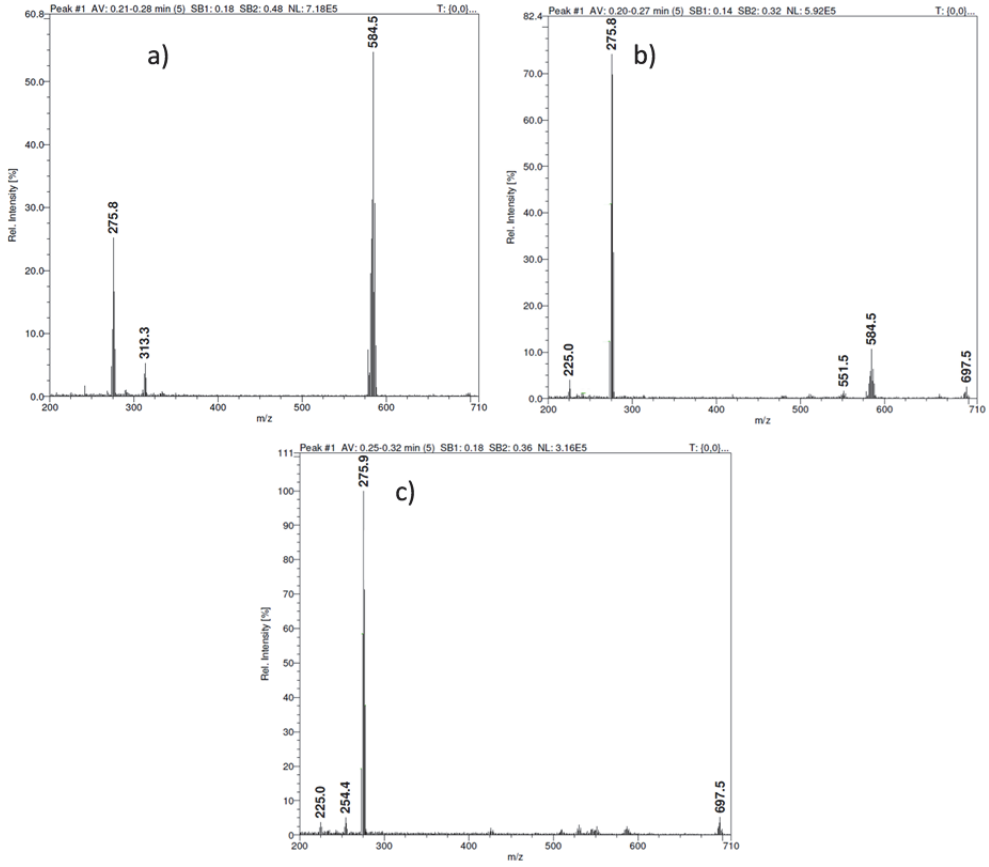

*Figure AIII.16. Mass spectra of a solution of [**3a**]PF_6 (0.062 mM) in water with a) 2% CH_3CN, b) 2% CH_3CN, and c) 80% CH_3CN after 15, 300, and 55 min irradiation, respectively, under Ar with a 493 nm LED with a photon flux of $1.13 \cdot 10^{-7} - 1.16 \cdot 10^{-7}$ mol·s^{-1} with peaks corresponding to $[Ru(dmbpy)_2(CH_3CN)_2]^{2+}$ (calcd m/z = 276.1), $\{[Ru(dmbpy)_2(L\text{-prol})(CH_3CN)] + H\}^{2+}$ (calcd m/z = 313.1), $[Ru(dmbpy)_2(L\text{-prol})]^{+}$ (calcd m/z = 584.2), $\{[Ru(dmbpy)_2(CH_3CN)_2]PF_6\}^{+}$ (calcd m/z = 697.1).*

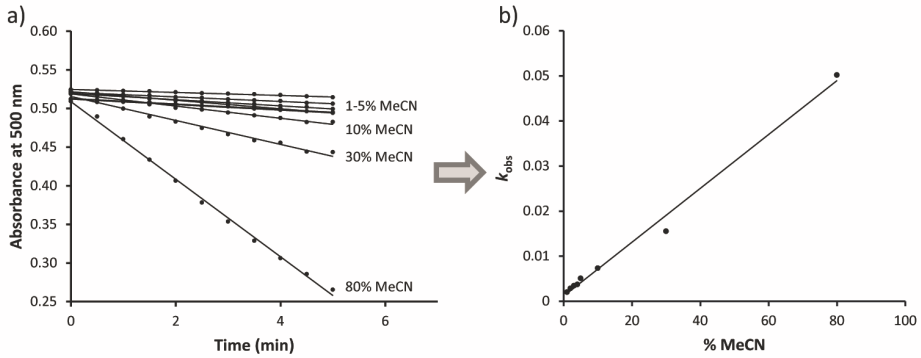

*Figure AIII.17. a) Plot of the evolution of the absorbance at 500 nm vs. time (first 5 min) during light irradiation of [**3a**]PF_6 in water containing different CH_3CN concentrations. Conditions: ruthenium concentration 0.062 mM, water contains 1, 2, 3, 4, 5, 10, 30, or 80 vol% CH_3CN, irradiation under Ar, light source is a 493 nm LED with a photon flux of $1.13 \cdot 10^{-7} - 1.16 \cdot 10^{-7}$ mol·s^{-1}. The negative slope of these curves is $-k_{obs}$. b) Evolution of k_{obs} vs. CH_3CN concentration (in vol%) in water. All the numerical values of k_{obs} are given in Table AIII.2.*

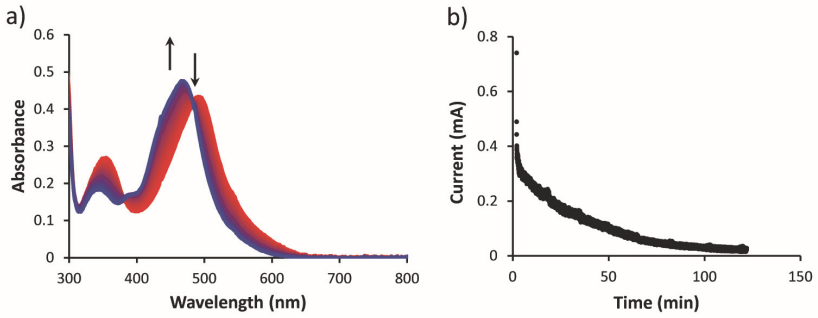

*Figure AIII.18. a) Evolution of the UV-vis spectra (region 350 – 650 nm) and b) current measured on the working electrode associated with the oxidation process vs. time during the electrochemical oxidation of a solution of [**1a**]PF_6 in PBS. Conditions: 0.1 mM [**1a**]PF_6 in PBS, carbon sponge working and counter electrodes, and Ag/AgCl reference electrode. Chronoamperometry was performed at +0.645 V and compartments were separated by a nafion membrane.*

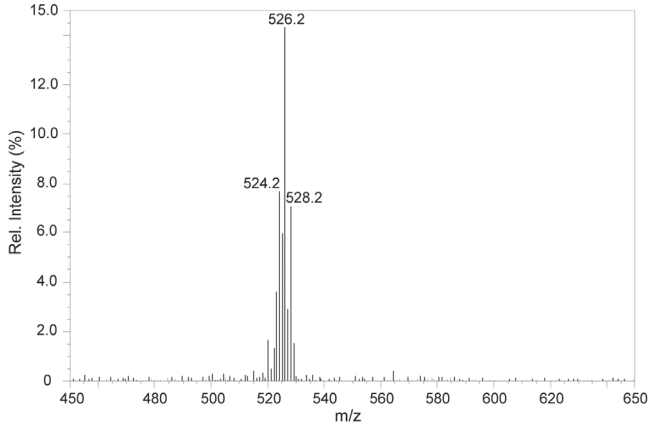

*Figure AIII.19. Mass spectrum after chronoamperometry of [**1a**]PF_6 in PBS with a peak corresponding to $[7]^+$ (calcd m/z = 526.1). Conditions: solution of [**1a**]PF_6 in PBS (0.1 mM), using carbon sponge as working and counter electrodes, and Ag/AgCl as a reference electrode. The experiment was performed at +0.645 V and compartments were separated by a nafion membrane.*

Table AIII.1. Conditions of the photoreactions monitored with MS, UV-vis, and CD.

Complex	Solvent	Stock solution			Working sol. (mM)	Photon flux 493 nm LED ($mol \cdot s^{-1}$)	Time (min)	Air /Ar
		w (mg)	V (mL)	M (mM)				
	PBS					$1.61 \cdot 10^{-7}$	180	Air
[**1a**]PF_6	PBS + 5 mM GSH	1.57	5	0.467	0.0178	$1.61 \cdot 10^{-7}$	180	Air
	PBS					$1.61 \cdot 10^{-7}$	150	Ar
[**2a**]PF_6	PBS	1.03	10	0.147	0.032	$1.19 \cdot 10^{-7}$	180	Air
[**2b**]PF_6	PBS	0.92	10	0.131	0.087	$1.09 \cdot 10^{-7}$	790	Air
[**3a**]PF_6	PBS	1.40	25	0.077	0.077	$1.48 \cdot 10^{-7}$	140	Air
[**1a**]PF_6	CH_3CN	0.96	10	0.142	0.071	$1.10 \cdot 10^{-7}$	90	Ar
[**2a**]PF_6	CH_3CN	1.29	10	0.184	0.092	$1.12 \cdot 10^{-7}$	80	Ar
[**2b**]PF_6	CH_3CN	1.28	10	0.182	0.121	$1.05 \cdot 10^{-7}$	70	Ar
[**3a**]PF_6	CH_3CN	1.08	10	0.148	0.074	$1.12 \cdot 10^{-7}$	180	Ar

*Table AIII.2. Observed rate constants (k_{obs}) for the formation of $[Ru(dmbpy)_2(CH_3CN)_2]^{2+}$ at different concentrations of CH_3CN. Conditions: solution of **[3a]**PF_6 (0.062 mM) in water with 1%, 2%, 3%, 4%, 5%, 10%, 30%, and 80% CH_3CN upon irradiation under Ar with a 493 nm LED with a photon flux of $1.13 \cdot 10^{-7} - 1.16 \cdot 10^{-7}$ mol·s^{-1}.*

vol% CH_3CN	k_{obs}
1	$2.03 \cdot 10^{-3}$
2	$2.86 \cdot 10^{-3}$
3	$3.43 \cdot 10^{-3}$
4	$3.72 \cdot 10^{-3}$
5	$5.08 \cdot 10^{-3}$
10	$7.34 \cdot 10^{-3}$
30	$1.55 \cdot 10^{-2}$
80	$5.02 \cdot 10^{-2}$

*Table AIII.3. Absolute and relative energies in water (COSMO) and dipole moments (D) of the isomers of **[1a]**$^+$, **[2b]**$^+$, and **[3a]**$^+$ optimized by DFT/PBE0/TZP.*

Isomer	Absolute energy in water (Hartree)	Relative energy ΔE in water (kJ.mol^{-1})	Dipole moment in water (debye)
[1a]$^+$	−16.77848092	0.0	37.8
[1b]$^+$	−16.77581705	6.9	52.5
[2a]$^+$	−18.22296593	1.9	11.1
[2b]$^+$	−18.22368686	0.0	35.8
[2c]$^+$	−18.21391701	25.7	73.1
[2d]$^+$	−18.22284318	2.2	53.7
[3a]$^+$	−19.67189354	0.0	34.7
[3b]$^+$	−19.66442602	19.6	52.0

*Table AIII.4. Calculated bond lengths (Å), angles (°), and structural distortion parameters in the DFT-minimized geometry of complexes **[1a]**$^{+}$, **[2b]**$^{+}$, and **[3a]**$^{+}$. Atom numbering is indicated in Figure AIII.20.*

Atoms	$[1a]^+$	$[2b]^+$	$[3a]^+$
Ru7-N15	2.1067	2.1080	2.1243
Ru7-N8	2.0802	2.0700	2.1035
Ru7-N21	2.0728	2.1268	2.1098
Ru7-N4	2.0798	2.1304	2.1175
Ru7-N34/N62	2.1650	2.1811	2.2111
Ru7-O48	2.1094	2.1055	2.1086
N4-Ru7-N21	78.39	78.49	78.29
N15-Ru7-N8	78.22	78.36	78.27
N34/62-Ru7-O48	80.21	79.84	78.02
N21-Ru7-N8	90.89	94.18	98.21
N4-Ru7-N8	95.21	95.36	101.4
N21-Ru7-N15	97.25	103.5	101.9
N21-Ru7-N34/62	96.86	94.43	97.92
N4-Ru7-N34/62	91.81	92.22	86.92
N4-Ru7-O48	94.55	99.05	98.26
N8-Ru7-O48	92.78	91.79	86.14
N15-Ru7-O48	90.11	79.57	81.58
N15-Ru7-N34/62	95.21	93.79	93.36
$^{a}\boldsymbol{\sigma^2}$	50.5	75.7	90.4
$^{b}\boldsymbol{\lambda}$	2.21	2.50	3.06

[a]The bond angle variance is $\sigma^2 = \frac{1}{11}\sum_{n=1,12}(\theta_n - 90)^2$*, where θn is one of the twelve angles in Table AIII.4. [b]The mean quadratic elongation is* $\lambda = \frac{1}{6}\sum_{n=1,6}\left[\frac{d_n - <d>}{<d>}\right]^2$*, where dn is one of the bond length in Table AIII.4 and <d> is the mean of those bond lengths.*

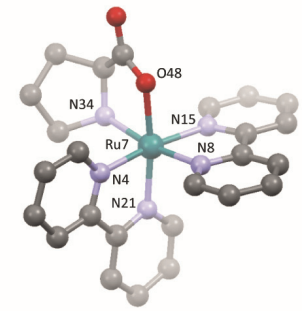

[1a]$^+$

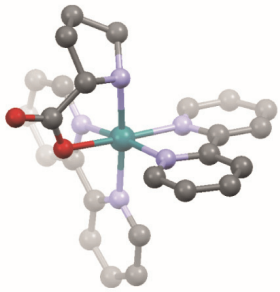

[1b]$^+$

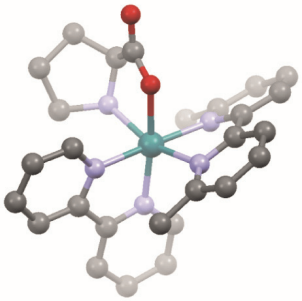

[2a]$^+$

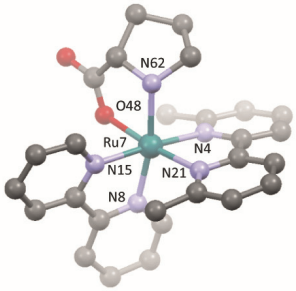

[2b]$^+$

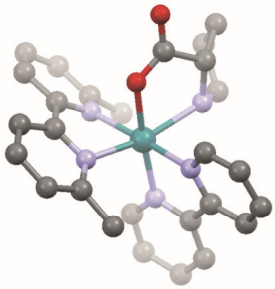

[2c]$^+$

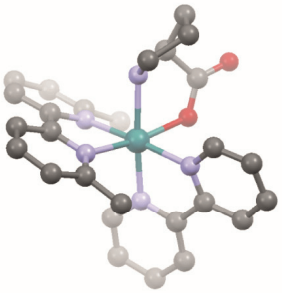

[2d]$^+$

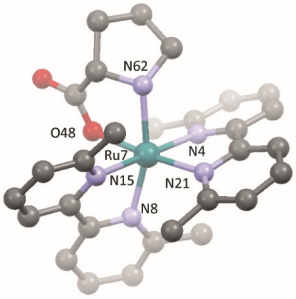

[3a]$^+$

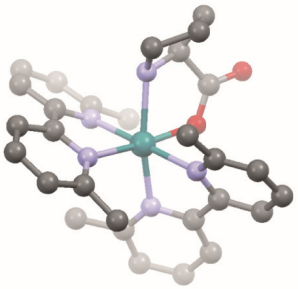

[3b]$^+$

*Figure AIII.20. Structures of **[1a]**$^+$, **[1b]**$^+$, **[2a]**$^+$, **[2b]**$^+$, **[2c]**$^+$, **[2d]**$^+$, **[3a]**$^+$, and **[3b]**$^+$ optimized by DFT in water (COSMO).*

APPENDIX IV: SUPPORTING INFORMATION FOR CHAPTER 3

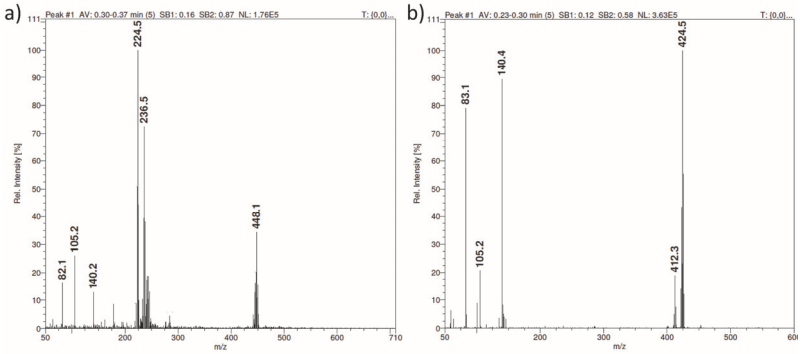

*Figure AIV.1. Mass spectrum of water solutions of (a) [**2**]Cl_2 and (b) [**3**]Cl_2 after 80 min irradiation with a 445 nm LED. a) Peaks corresponding to {mtmp + H}$^+$ (calcd m/z = 140.2), $[Ru(bpy)_2(OH_2)_2]^{2+}$ (calcd m/z = 225.0), $[Ru(bpy)_2(OH_2)(OH)]^+$ (calcd m/z = 448.5). b) Peaks corresponding to {mtmp + H}$^+$ (calcd m/z = 140.2) and $[Ru(Ph_2phen)_2(CH_3CN)_2]^{2+}$ (calcd m/z = 424.1). Conditions are detailed in Figure 3.1.*

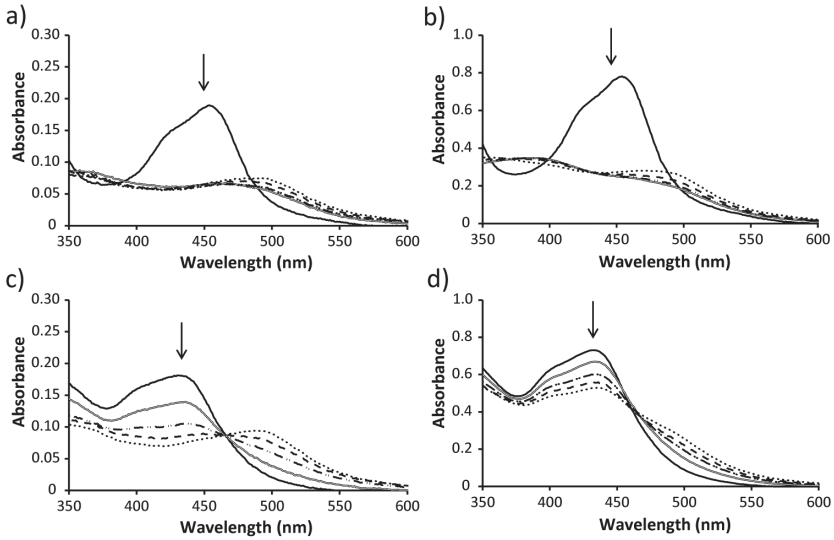

*Figure AIV.2. Evolution of the UV-vis spectrum of a well in a 96-well plate containing compound (a) [**1**]Cl_2 (40 μM), (b) [**1**]Cl_2 (200 μM), (c) [**2**]Cl_2 (40 μM), and (d) [**2**]Cl_2 (200 μM) in OptiMEM complete, under blue light irradiation (310 K) at 0 min (—), 2 min (=), 5 min (—·· —), 8 min (- - -), 10 min (···). Under such conditions, 10 min irradiation correspond to a light dose of 6.5 J·cm^{-2}*

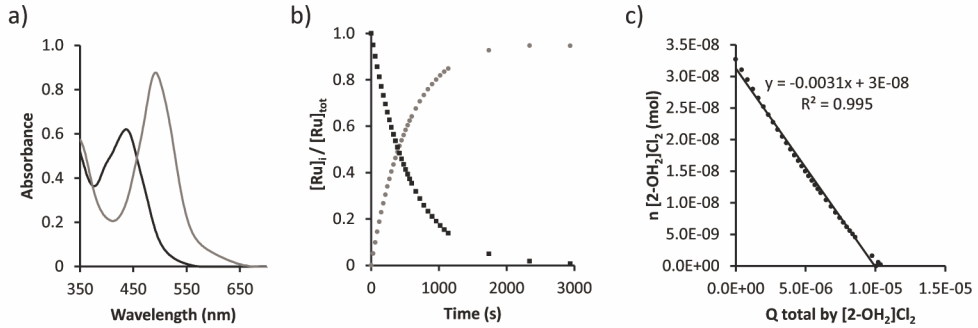

*Figure AIV.3. Kinetic data for the second step of the photosubstitution of [**2**]Cl_2 in water under N_2. a) Globally fitted absorption spectra of the mono-aqua intermediate [Ru(bpy)$_2$(η^1-mtmp)(OH_2)]Cl_2 ([**2**-OH_2]Cl_2, black) and [Ru(bpy)$_2$(OH_2)$_2$]Cl_2 (grey) according to modelling using the Glotaran software. b) Modelled evolution of the relative concentrations of [**2**-OH_2]Cl_2 (squares) and [Ru(bpy)$_2$(OH_2)$_2$]Cl_2 (circles) vs. irradiation time according to global fitting using Glotaran. c) Plot of the amount of [**2**-OH_2]Cl_2 (mol) vs. total amount of photons absorbed by [**2**-OH_2]Cl_2 (mol). The slope of the obtained line is the opposite of the quantum yield of the formation of the bis-aqua complex. Conditions: 0.109 mM solution of [**2**-OH_2]Cl_2 in demineralized water irradiated at 298 K under N_2 using a 445 nm LED at $1.49 \cdot 10^{-7}$ mol·s^{-1}.*

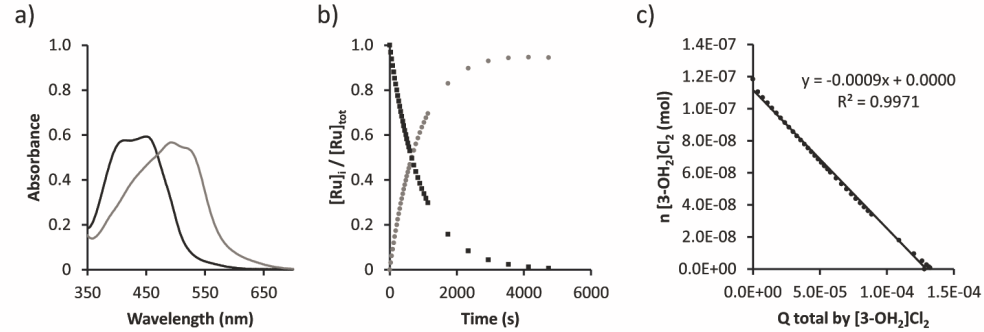

*Figure AIV.4. Kinetic data for the second step of the photosubstitution of [**3**]Cl_2 in water under N_2. a) Globally fitted absorption spectra of the mono-aqua intermediate [Ru(Ph_2phen)$_2$(η^1-mtmp)(OH_2)]Cl_2 ([**3**-OH_2]Cl_2, black) and [Ru(Ph_2phen)$_2$(OH_2)$_2$]Cl_2 (grey) according to modelling using the Glotaran software. b) Modelled evolution of the relative concentrations of [**3**-OH_2]Cl_2 (squares) and [Ru(Ph_2phen)$_2$(OH_2)$_2$]Cl_2 (circles) vs. irradiation time according to global fitting using Glotaran. c) Plot of the amount of [**3**-OH_2]Cl_2 (mol) vs. total amount of photons absorbed by [3-OH_2]Cl_2 (mol). The slope of the obtained line is the opposite of the quantum yield of the formation of the bis-aqua complex. Conditions: 0.038 mM solution of [**3**-OH_2]Cl_2 in demineralized water irradiated at 298 K under N_2 using a 445 nm LED at $1.31 \cdot 10^{-7}$ mol·s^{-1}.*

APPENDIX V: SUPPORTING INFORMATION FOR CHAPTER 4

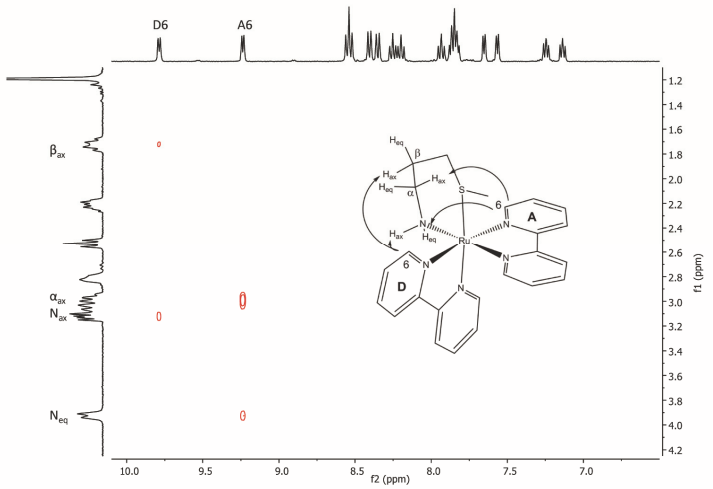

*Figure AV.1. NOESY NMR spectrum of a solution of **[1]**$(PF_6)_2$ in D_2O showing off-diagonal peaks between the α_{ax} proton and the A6 proton, the N_{eq} proton and the A6 proton, the β_{ax} proton and the D6 proton, and the N_{ax} proton and the D6 proton. This confirms that the isomer is Λ-(S)-eq-**[1]**$^{2+}$.*

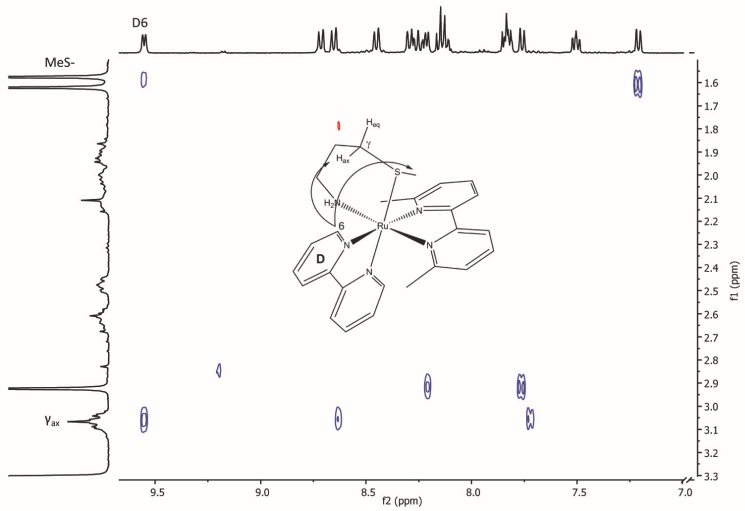

*Figure AV.2. NOESY NMR spectrum of a solution of **[2]**$(PF_6)_2$ in CD_3OD showing off-diagonal peaks between the γ_{ax} proton and the D6 proton, and the methyl thioether group and the D6 proton. This confirms that the isomer is Λ-(R)-eq-**[2a]**$^{2+}$.*

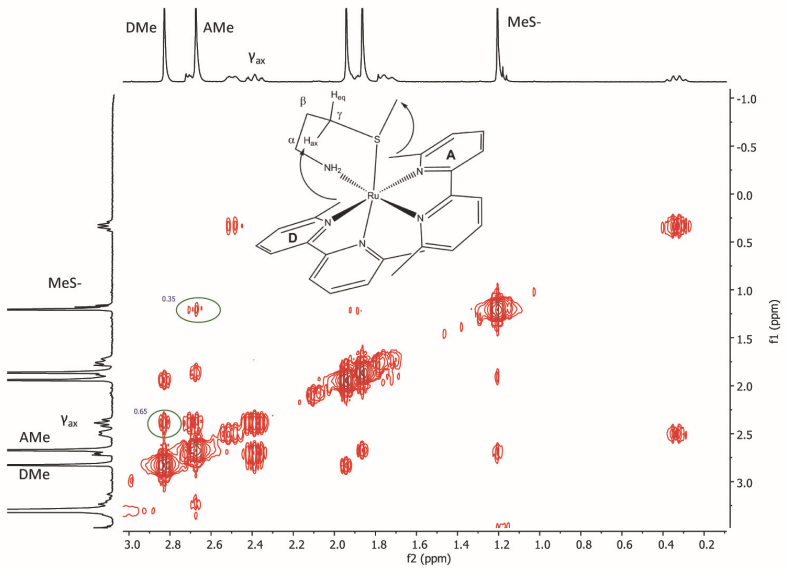

*Figure AV.3. NOESY NMR spectrum of a solution of **[3]**$(PF_6)_2$ in CD_3OD showing off-diagonal peaks between the γ_{ax} proton and the DMe substituent, and the methyl thioether group and the AMe substituent, with relatives intensities of 65% and 35% respectively. This confirms that the isomer is Λ-(S)-ax-**[3]**$^{2+}$.*

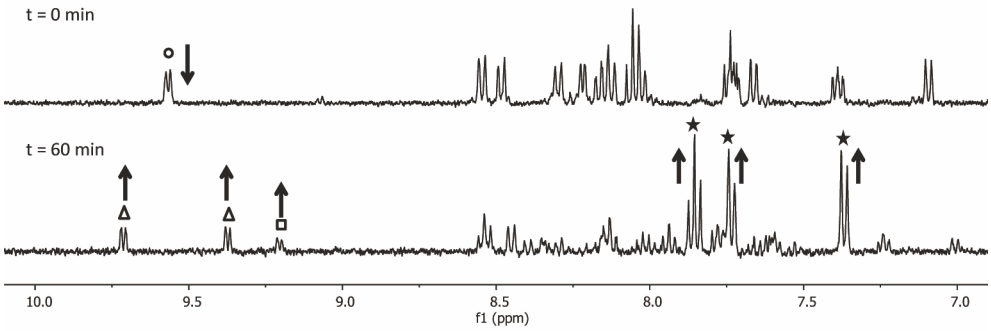

*Figure AV.4. Evolution of the ^{1}H NMR spectra (region 10 – 7 ppm) of a solution of **[2]**$(PF_6)_2$ in D_2O irradiated under N_2 with a Xe lamp at 298 K. The doublet at 9.57 ppm (triangle) corresponds to the H_6 proton on the bpy for complex **[2]**$^{2+}$ (circle) and the rising doublets at 9.72, 9.38, and 9.21 ppm correspond to the H_6 proton on the bpy of two new complexes (triangles and square). The arising peaks at 7.86, 7.74, and 7.37 ppm correspond to free dmbpy (star). Concentration of **[2]**$(PF_6)_2$ = 1.99 mM.*

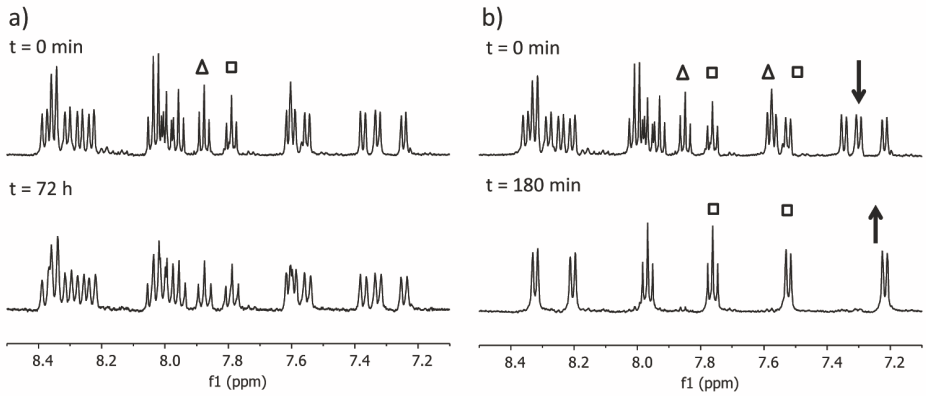

*Figure AV.5. a) Evolution of the ^{1}H NMR spectra (region 8.5 – 7.2 ppm) of a solution of **[3]**$(PF_6)_2$ at 298 K in D_2O under N_2 in the dark. No change in the spectra is observed. b) Evolution of the ^{1}H NMR spectra (region 8.5 – 7.2 ppm) of a solution of **[3]**$(PF_6)_2$ in D_2O irradiated under N_2 with a Xe lamp at 298 K. Peaks with a triangle corresponds to **[3]**$(PF_6)_2$ and peaks with a square correspond to $[Ru(dmbpy)_2(OH_2)]^{2+}$. Concentration of **[3]**$(PF_6)_2$ = 2.61 mM.*

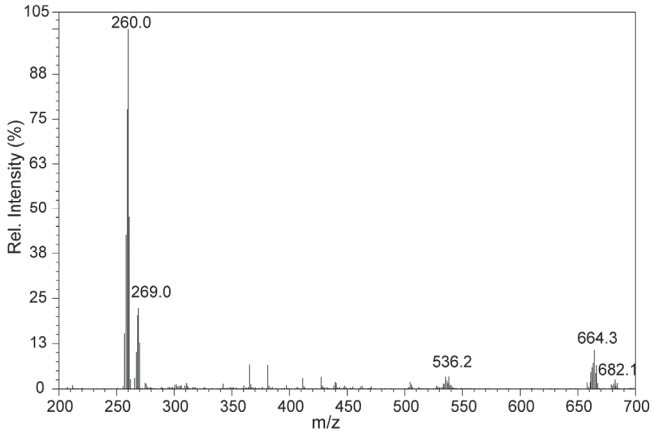

*Figure AV.6. Mass spectrum of a 0.145 mM solution of **[1]**$(PF_6)_2$ in water after 6 min of light irradiation at 298 K with a 445 nm LED with a photon flux of $2.98 \cdot 10^{-8}$ mol·s^{-1} under N_2 with peaks corresponding to $[Ru(bpy)_2(mtpa)]^{2+}$ (calcd m/z = 259.6), $[Ru(bpy)_2(mtpa)(OH_2)]^{2+}$ (calcd m/z = 268.6), and $[Ru(bpy)_2(mtpa)(OH)]^{+}$ (calcd m/z = 536.1). Conditions are detailed in Table 4.5.*

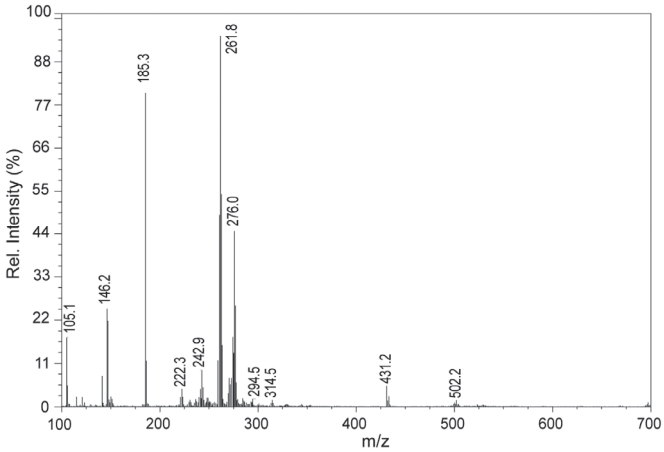

*Figure AV.7. Mass spectrum of a 0.101 mM solution of **[2]**$(PF_6)_2$ in water after 60 min of light irradiation at 298 K with a 445 nm LED with a photon flux of $2.92 \cdot 10^{-8}$ mol·s^{-1} under N_2 with peaks corresponding to {mtpa + H}$^+$ (calcd. m/z = 106.1), {dmbpy + H} (calcd m/z = 185.2), [Ru(dmbpy)(bpy)$(CH_3CN)_2]^{2+}$ (calcd m/z = 262.1), and [Ru(bpy)(mtpa)$(CH_3CN)_2]^{2+}$ (calc. m/z = 222.5). Conditions are detailed in Table 4.5.*

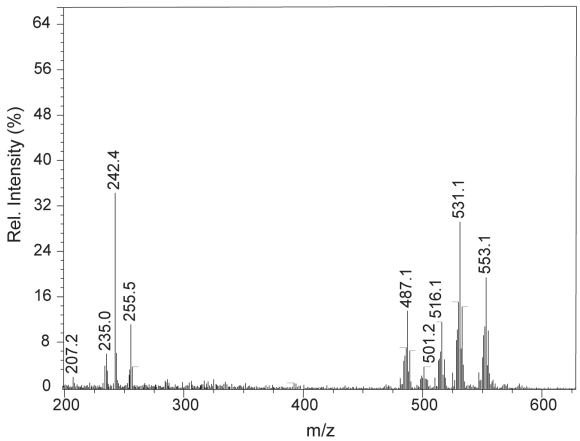

*Figure AV.8. Mass spectrum of a 0.123 mM solution of **[3]**$(PF_6)_2$ in water after light irradiation at 298 K with a 445 nm LED with a photon flux of $2.79 \cdot 10^{-7}$ mol·s^{-1} under N_2 with no peaks corresponding to tha starting **[3]**$(PF_6)_2$. Conditions are detailed in Table 4.5.*

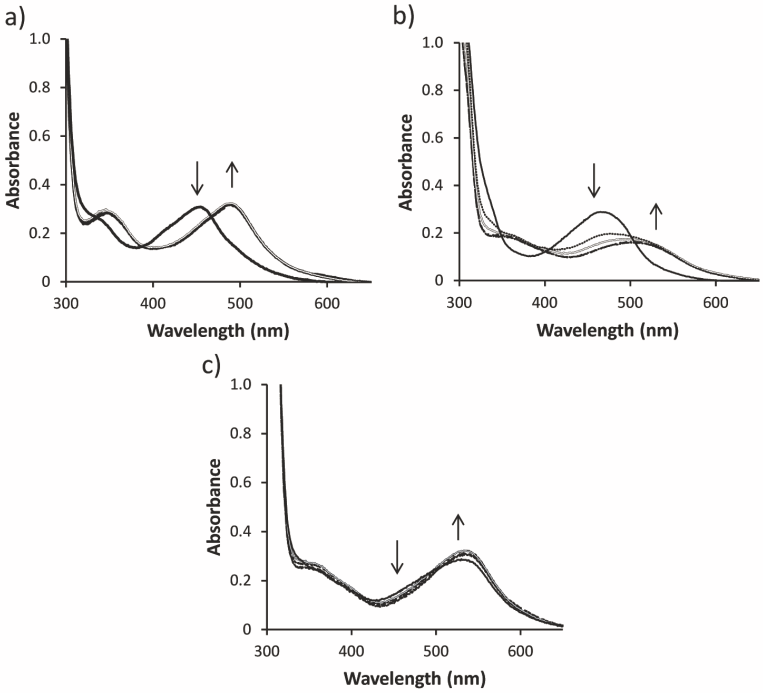

*Figure AV.9. Evolution of the UV-vis spectra of a well in a 96-well plate containing compound (a) [**1**](PF$_6$)$_2$ (86 μM), (b) [**2**](PF$_6$)$_2$ (86 μM), or (c) [**3**](PF$_6$)$_2$ (86 μM) in OptiMEM complete under blue light irradiation (37 °C) at 0 min (—), 2 min (···), 5 min (=), 10 min (- - -), or 15 min (—·· —).*

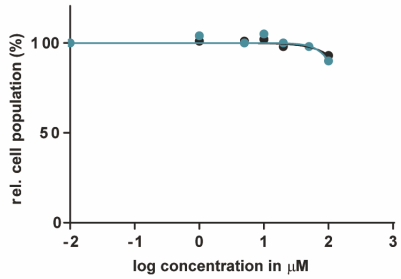

Figure AV.10. Dose-response curves for A549 cells in presence of mtpa irradiated with blue light (454 nm, 6.35 J·cm^{-2}) 6 h after treatment (blue data points) or left in the dark (black data points). Photocytotoxicity assay outline: cells seeded at 5·10^3 cells/well at t = 0 h, treated with mtpa at t =24 h, irradiated at t = 30 h, and SRB cell-counting assay performed at t = 96 h. Incubation conditions: 37 °C and 7% CO$_2$.

*Table AV.1. Calculated bond lengths (Å), angles (°), and structural distortion parameters in the DFT-minimized geometry of complexes **[1]**$^{2+}$, **[2]**$^{2+}$, and **[3]**$^{2+}$.*

Atoms	Λ-(*R*)-*eq*-[**1**]$^{2+}$	Λ-(*S*)-*eq*-[**1**]$^{2+}$	Λ-(*R*)-*eq*-[**2a**]$^{2+}$	Λ-(*S*)-*eq*-[**2a**]$^{2+}$	Λ-(*R*)-*eq*-[**2b**]$^{2+}$	Λ-(*S*)-*eq*-[**2b**]$^{2+}$	Λ-(R)-*eq*-[**3**]$^{2+}$	Λ-(*S*)-*eq*-[**3**]$^{2+}$	Λ-(*S*)-*ax*-[**3**]$^{2+}$
Ru13-N12	2.106	2.102	2.156	2.162	2.104	2.109	2.155	2.194	2.144
Ru13-N3	2.093	2.093	2.148	2.154	2.104	2.164	2.129	2.146	2.129
Ru13-N21	2.098	2.107	2.088	2.086	2.16	2.101	2.125	2.156	2.130
Ru13-N14	2.111	2.115	2.109	2.101	2.187	2.181	2.136	2.201	2.144
Ru13-N26	2.169	2.181	2.177	2.174	2.172	2.183	2.194	2.207	2.186
Ru13-S30	2.384	2.368	2.407	2.414	2.397	2.372	2.438	2.366	2.427
N12-Ru13-N3	77.92	77.93	77.48	77.54	77.8	77.48	77.44	76.67	77.51
N21-Ru13-N14	77.73	77.78	77.89	77.91	76.94	77.13	77.50	76.34	77.35
N26-Ru13-S30	90.31	91.54	89	91.02	93.04	90.99	81.74	91.17	86.78
N12-Ru13-N21	95.12	94.6	96.62	96.07	94.45	95.48	100.67	89.22	100.46
N3-Ru13-N21	89.39	89.69	93.95	94.68	86.59	87.48	96.70	86.06	97.03
N3-Ru13-N14	95.79	96.24	102.24	101.25	92.09	91.87	101.67	90.33	100.86
N3-Ru13-S30	92.6	91.47	87.64	86.27	88.6	91.29	94.90	91.59	89.26
N12-Ru13-S30	83.6	93.76	83.06	90.75	79.33	88.83	77.89	93.39	84.51
N12-Ru13-N26	98.82	99.29	99.69	99.77	98.42	101.86	98.70	107.51	98.98
N14-Ru13-S30	103.79	93.84	102.45	95.26	108.56	90.31	104.12	100.46	97.84
N14-Ru13-N26	87.03	86.13	80.88	81.72	91.32	88.51	82.28	84.89	82.80
N21-Ru13-N26	87.61	87.71	89.38	88.34	91.39	98.23	86.45	90.93	87.15
[a]σ^2	62.4	45.0	81.8	63.3	81.8	52.5	108.6	76.3	76.0
[b]λ	0.0022	0.0020	0.0023	0.0025	0.0021	0.0017	0.0029	0.0017	0.0027

[a]The bond angle variance is $\sigma^2 = \frac{1}{11}\sum_{n=1,12}(\theta_n - 90)^2$*, where* θ_n *is one of the twelve angles in Table AV.1.* *[b]The mean quadratic elongation is* $\lambda = \frac{1}{6}\sum_{n=1,6}\left[\frac{d_n - <d>}{<d>}\right]^2$*, where* d_n *is one of the bond length in Table AV.1 and <d> is the mean of those bond lengths.*

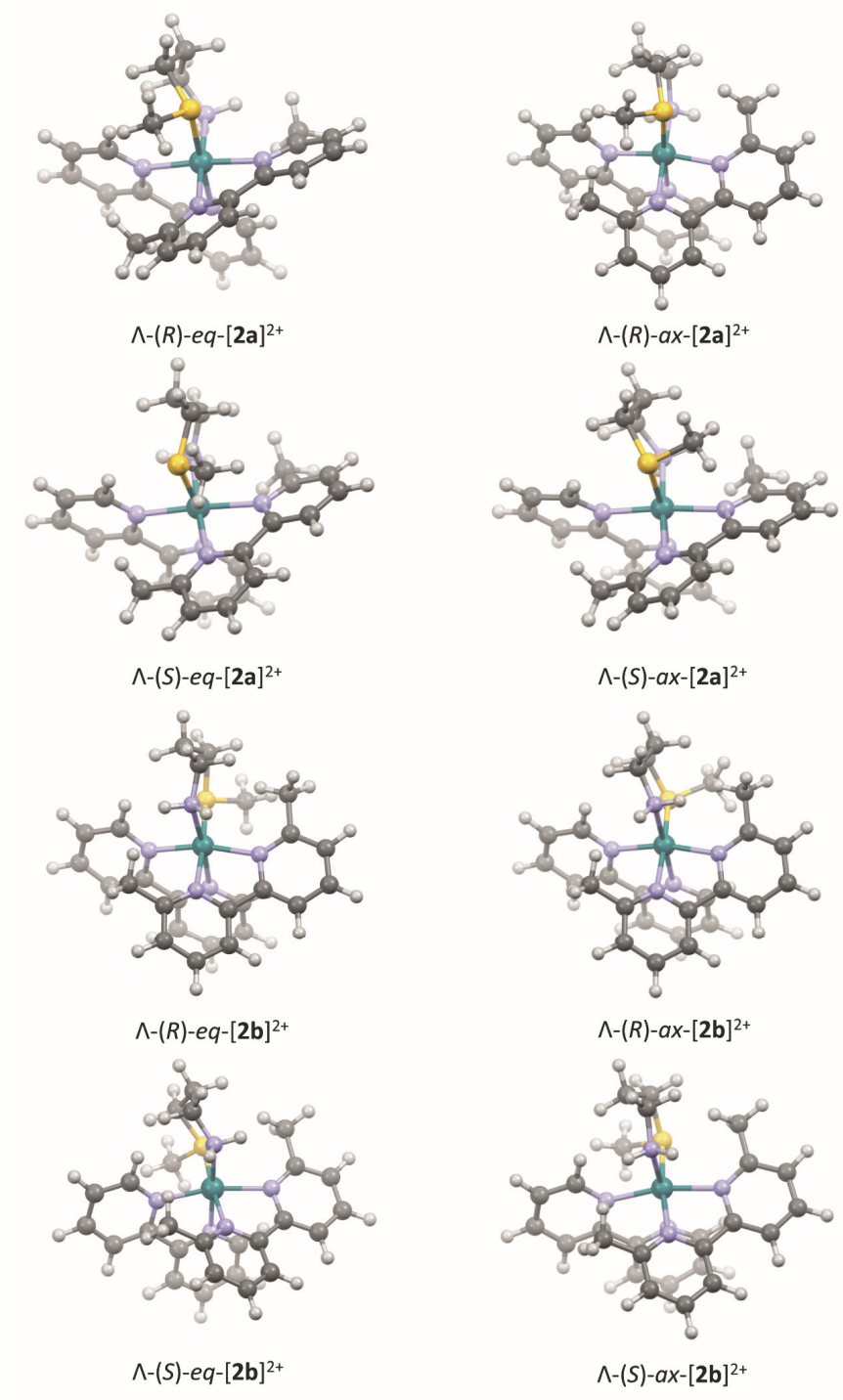

Figure AV.11. Structures of the isomers of $[\mathbf{2}]^{2+}$ *optimized by DFT in water (COSMO).*

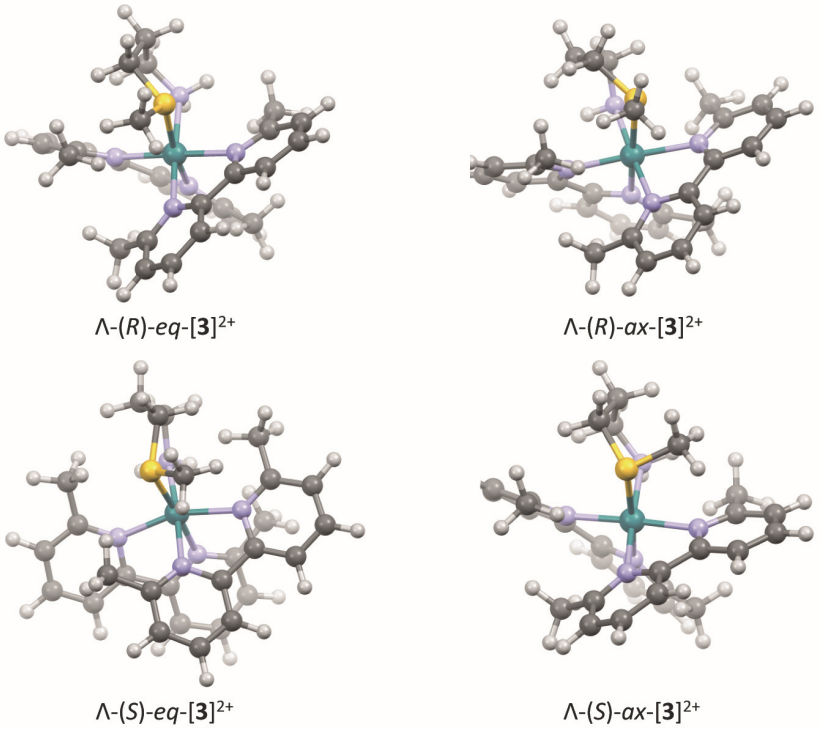

*Figure AV.12. Structures of the isomers of [**3**]$^{2+}$ optimized by DFT in water (COSMO).*

APPENDIX VI: SUPPORTING INFORMATION FOR CHAPTER 5

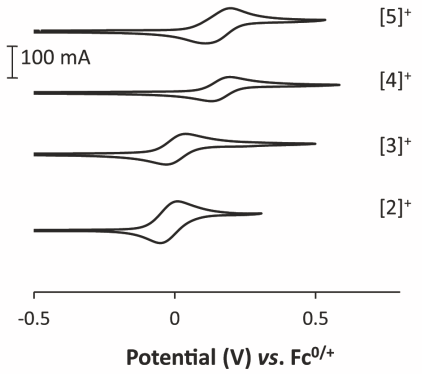

*Figure AVI.1. Cyclic voltammograms of 1 mM solutions of [**2**]PF_6, [**3**]PF_6, [**4**]PF_6, and [**5**]PF_6 in 0.1 M Bu_4NPF_6/CH_3CN (v = 100 $mV \cdot s^{-1}$).*

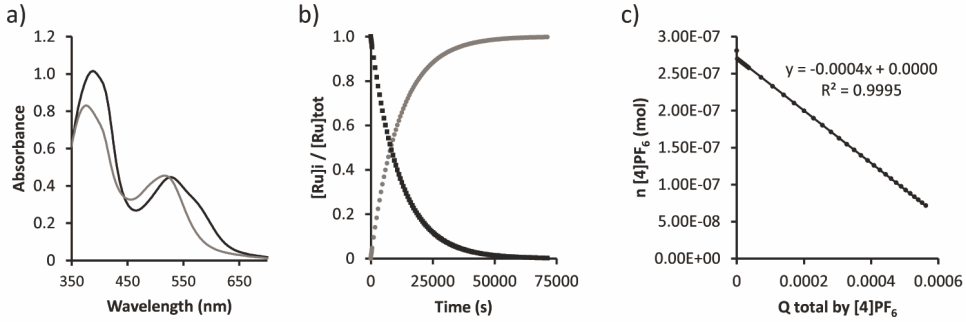

*Figure AVI.2. Kinetic data for the photosubstitution of [**4**]PF_6 in CH_3CN under N_2. a) Left axis: globally fitted absorption spectra of [**4**]PF_6 (black) and [Ru(bpy)(phpy)$(CH_3CN)_2$]PF_6 (grey) according to modelling using the Glotaran software. b) Modelled evolution of the relative concentrations of [**4**]PF_6 (squares) and [Ru(bpy)(phpy)$(CH_3CN)_2$]PF_6 (circles) vs. irradiation time according to global fitting using Glotaran. c) Plot of the amount of [**4**]PF_6 (mol) vs. total amount of photons absorbed by [**4**]PF_6 (mol). The slope of the obtained line is the opposite of the quantum yield of the formation of the bis-acetonitrile complex. Conditions: 0.094 mM solution of [**4**]PF_6 in CH_3CN irradiated at 298 K under N_2 using a 521 nm LED at $6.80 \cdot 10^{-8}$ $mol \cdot s^{-1}$.*

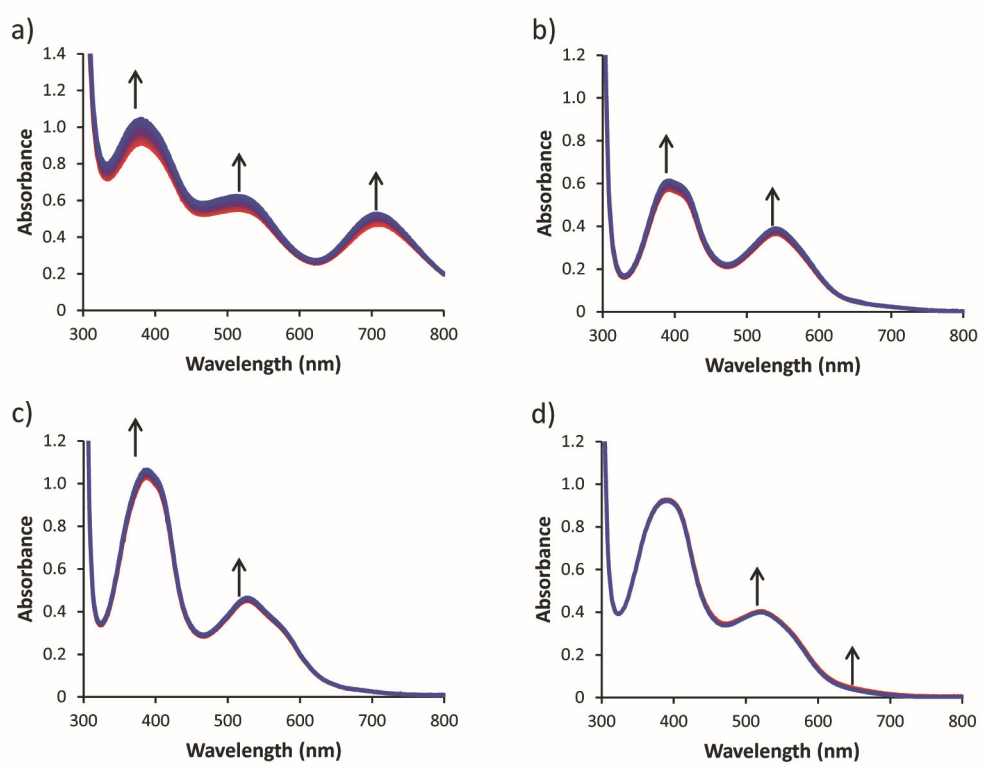

*Figure AVI.3. Evolution of the UV-vis spectra over 10 h in the dark at room temperature and under air of acetonitrile solutions of a) **[2]**PF_6, b) **[3]**PF_6, c) **[4]**PF_6, and d) **[5]**PF_6.*

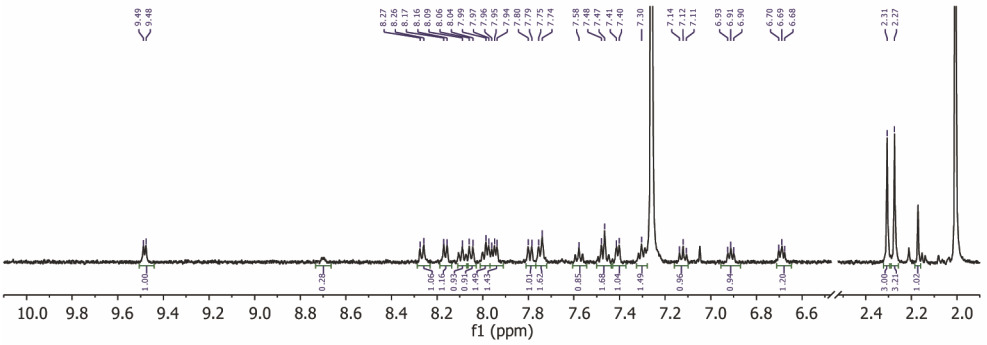

*Figure AVI.4. ^{1}H NMR of a solution of **[1b]**PF_6 in $CDCl_3$. After irradiation of **[1a]**PF_6 in CH_3CN with a Xe lamp mounted with a <400 nm filter and an IR filter, the solvent was evaporated and the photoproduct was redissolved in $CDCl_3$.*

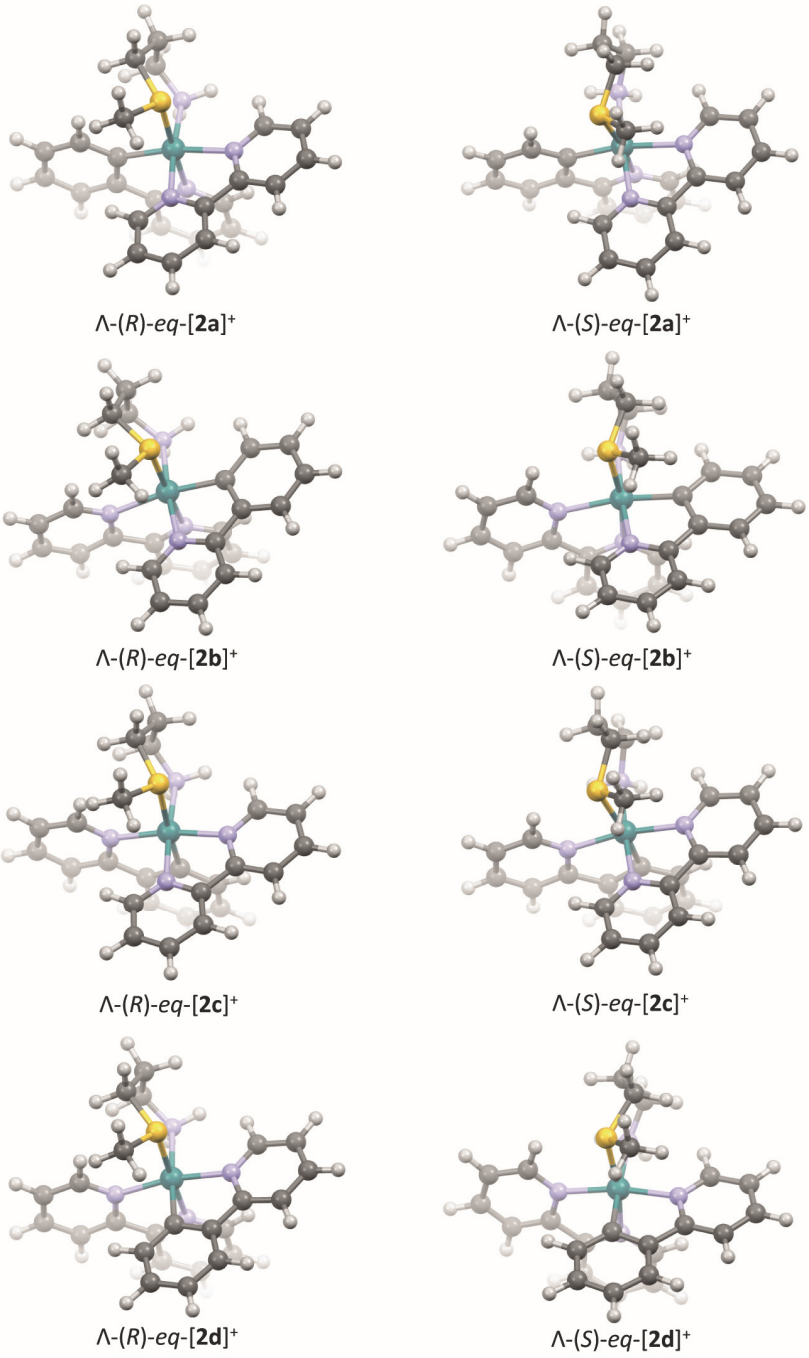

*Figure AVI.5. Structures of isomers Λ-(R)-eq and Λ-(S)-eq of **[2a]**$^+$, **[2b]**$^+$, **[2c]**$^+$, and **[2d]**$^+$ optimized by DFT in water (COSMO).*

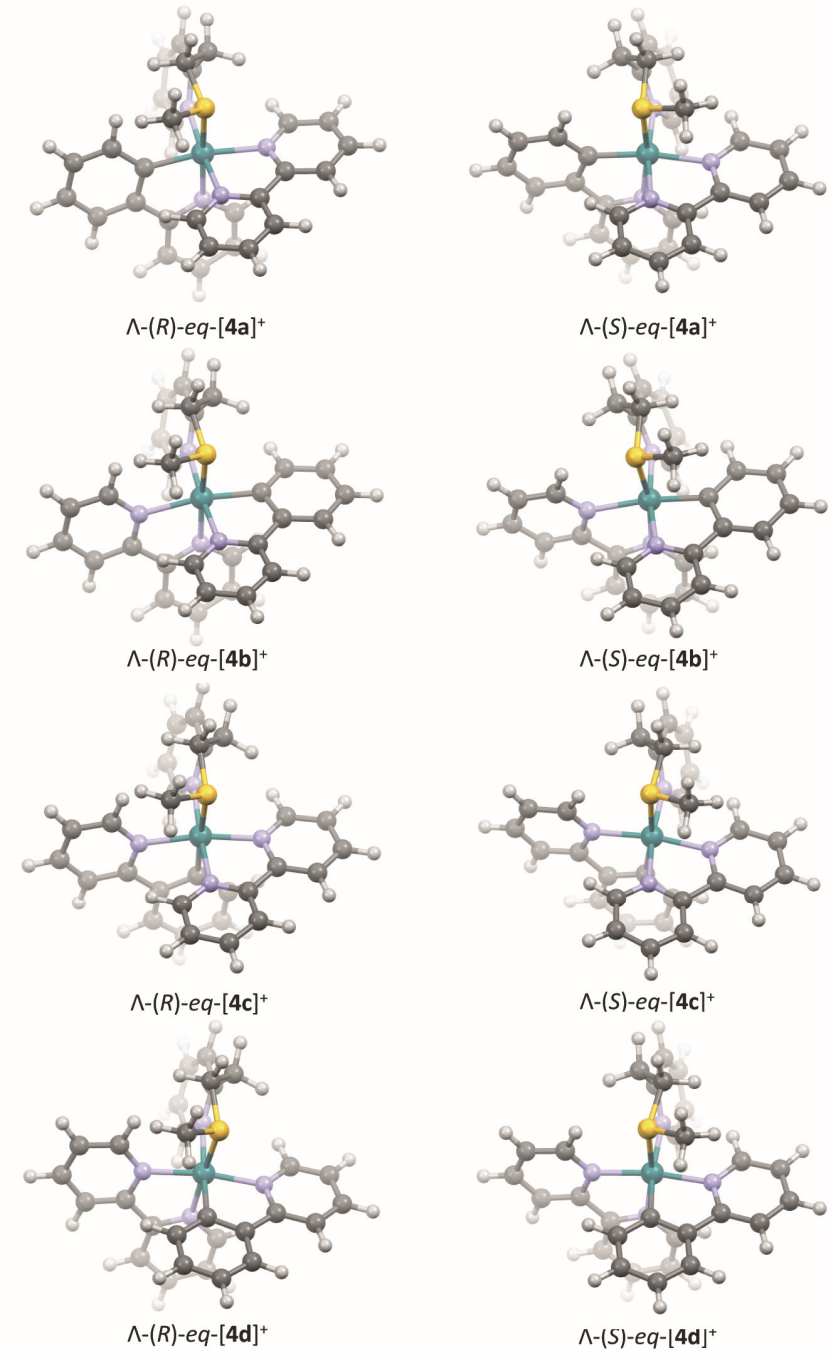

*Figure AVI.6. Structures of isomers Λ-(R)-eq and Λ-(S)-eq of **[4a]**$^{+}$, **[4b]**$^{+}$, **[4c]**$^{+}$, and **[4d]**$^{+}$ optimized by DFT in water (COSMO).*

APPENDIX VII: SUPPORTING INFORMATION OF CHAPTER 6

AVII.1 Comments on the synthesis

Due to the dissymmetry of mtmp, two different coordination isomers were obtained for [Ru(Ph_2phen)(mtmp)(ox)] ([**8**]): one with the sulfur donor *trans* to Ph_2phen, and another one with the sulfur donor atom *trans* to ox^{2-}. These two isomers can be separated by column chromatography on alumina using a mixture CH_2Cl_2:CH_3OH as eluent. However, when working with a pure isomer, further replacement of the ox^{2-} by bpy yielded a mixture of two isomers of *cis*-[Ru(Ph_2phen)(bpy)(mtmp)]$(PF_6)_2$ ([**2**]$(PF_6)_2$) that probably have the sulfur atom either *trans* to Ph_2phen or to bpy. As isomerization occurred as well in this last step, the isolation of pure isomers of [**8**] was later avoided, keeping a single separation step after coordination of the third ligand, *i.e.* after $[\mathbf{2}]^{2+}$ was obtained.

Full characterization of $[\mathbf{2b}]^{2+}$ was attempted using 2D NMR (NOESY) spectroscopy in CD_3CN. Off-diagonal correlations were observed between one of the H_β protons and B6, and between the other H_β and P1 (Figure AVII.1). Thus, these signals are not conclusive and may correspond either to the isomer with the sulfur donor *trans* to bpy or the isomer with the sulfur donor *trans* to Ph_2phen Unfortunately, no other off-diagonal correlation peak involving the thiomethyl group was observed, which prevents from unambiguously assigning $[\mathbf{2b}]^{2+}$ as the isomer with S *trans* to bpy or to Ph_2phen. Probably, the methyl group sits above the middle of both the bpy or the Ph_2phen ligands, as shown in Chapter 4 for similar complexes. Unfortunately, single crystals suitable for X-Ray crystallography could not be obtained.

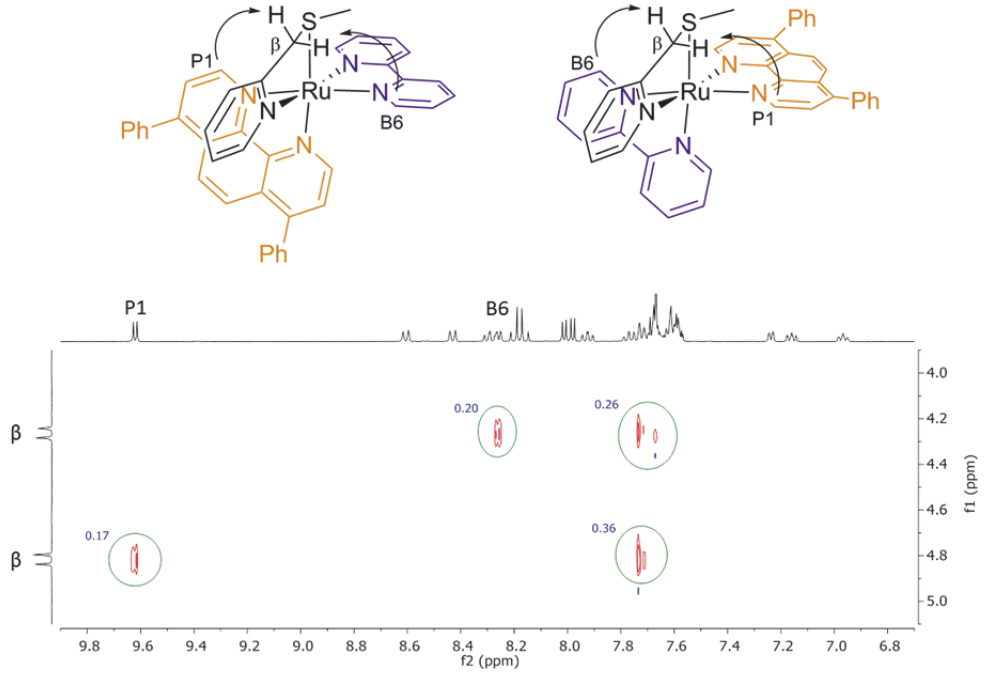

*Figure AVII.1. NOESY NMR spectrum of a solution of a purified isomer of **[2]**$(PF_6)_2$, called **[2b]**$(PF_6)_2$, in CD_3CN. Off-diagonal peaks between one of the H_β of mtmp and B6 and between the other H_β and P1 can be seen, with relative intensities of 20% and 17%, respectively. The other interaction (36% and 26%) corresponds to off-diagonal correlations correspond to intraligand NOESY interactions.*

Table AVII.1. Selected bond length (Å) and angles (°) for Λ-(S)/Δ-(R)-[Ru(dmbpy)$_2$(mtmp-κN,κS)]Cl_2·CH_3OH·H_2O.

	Λ-(*S*)-[3]Cl_2
Ru1-S1	2.3709(4)
Ru1-N1	2.1254(12)
Ru1-N2	2.0928(12)
Ru1-N3	2.0934(12)
Ru1-N4	2.1000(12)
Ru1-C5	2.1362(12)
S1-C30-C29-N5	−26.36(16)

AVII.2 Photochemistry

Due to the different solubility in water of the four complexes, their photochemistry was described either in water or in acetonitrile. In Chapter 2 we already highlighted the importance of the solvent on photosubstitution reactions. In order to assess whether

photosubstitution would happen during photocytotoxicity assays, solutions of [**1**]Cl_2, [**2**]$(PF_6)_2$, [**3**]Cl_2, [**4**]PF_6, and [**5**]Cl_2 in the cell culture media containing less than 0.5% DMSO were irradiated with green light (520 nm) in a 96-well plate using the irradiation setup of the cell assay.

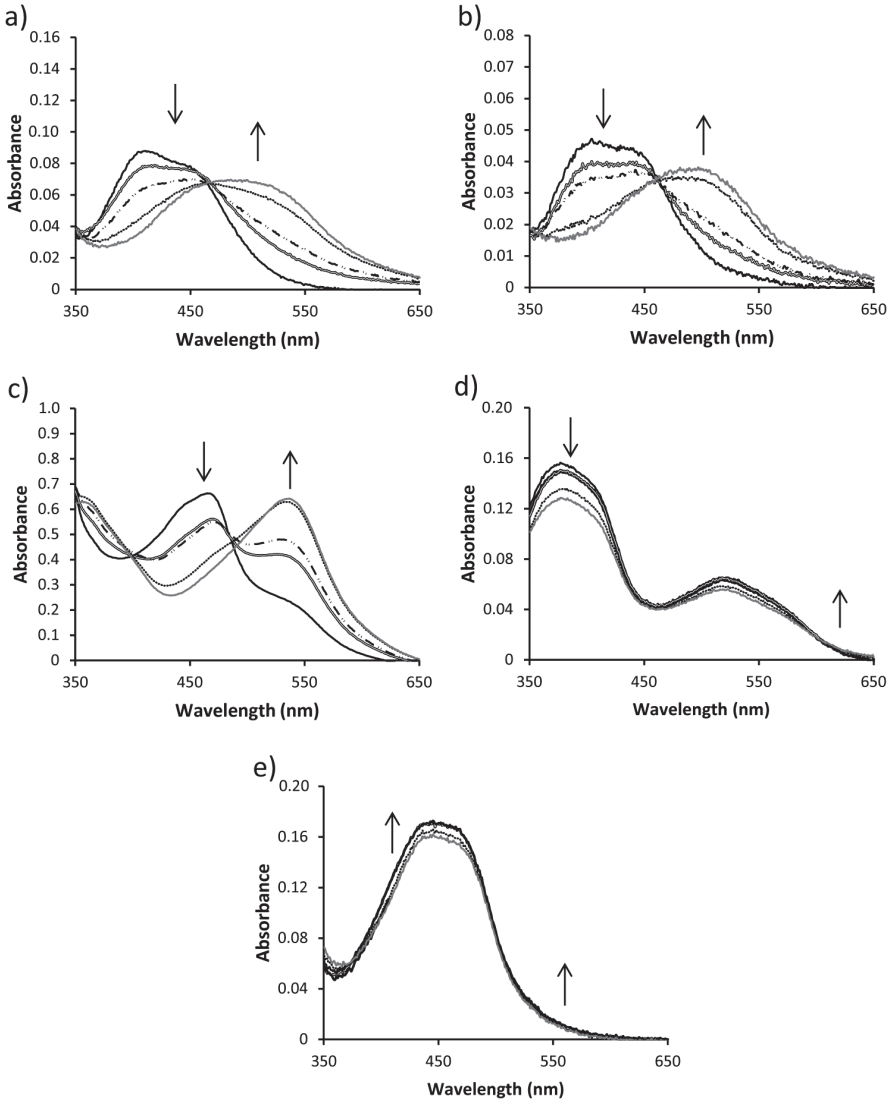

*Figure AVII.2. Evolution of the UV-vis spectrum of a well in a 96-well plate containing compound (a) [**1**]Cl_2 (20 µM), (b) [**2**]$(PF_6)_2$ (20 µM), (c) [**3**]Cl_2 (200 µM), (d) [**4**]PF_6 (10 µM), and e) [**5**]Cl_2 (20 µM) in OptiMEM complete, under green light irradiation (37 °C) at 0 min (continuous black), 2 min (=), 5 min (—·· —),15 min (···), and 30 min (continuous grey). In such conditions, 15 min irradiation correspond to a light dose of 18.8 J.cm^{-2}.*

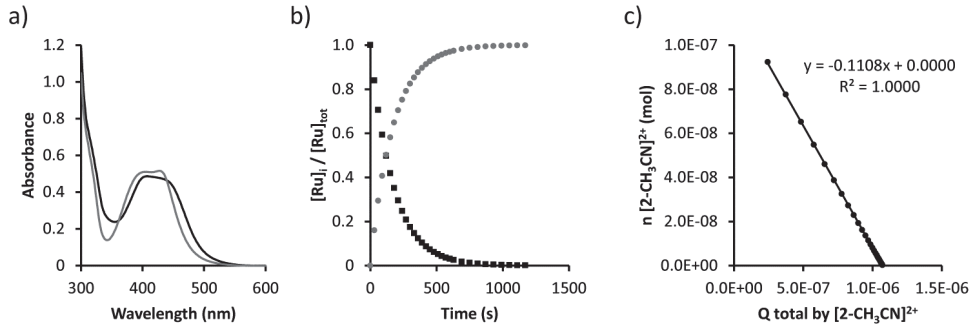

Figure AVII.3. Kinetic data for the second step of the photosubstitution of ***[2]***$(PF_6)_2$ *in* CH_3CN *under* N_2*. a) Globally fitted absorption spectra of the mono-aqua intermediate* $[Ru(bpy)(Ph_2phen)(\eta^1\text{-mtmp})(CH_3CN)]^{2+}$ ($[\mathbf{2}\text{-}CH_3CN]^{2+}$*, black) and* $[Ru(Ph_2phen)_2(CH_3CN)_2]^{2+}$ *(grey) according to modelling using the Glotaran software. b) Modelled evolution of the relative concentrations of* $[\mathbf{2}\text{-}CH_3CN]^{2+}$ *(squares) and* $[Ru(Ph_2phen)_2(CH_3CN)_2]^{2+}$ *(circles) vs. irradiation time according to global fitting using Glotaran. c) Plot of the amount of* $[\mathbf{2}\text{-}CH_3CN]^{2+}$ *(mol) vs. total amount of photons absorbed by* $[\mathbf{2}\text{-}CH_3CN]^{2+}$ *(mol). The slope of the obtained line is the opposite of the quantum yield of the formation of the bis-aqua complex. Conditions: 0.036 mM solution of* ***[2]***$(PF_6)_2$ *in* CH_3CN *irradiated at 298 K under* N_2 *using a 521 nm LED at* $6.21 \cdot 10^{-8}$ $mol \cdot s^{-1}$.

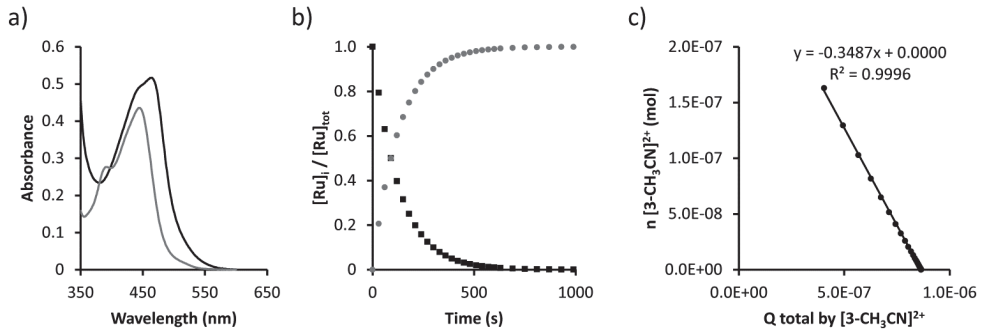

Figure AVII.4. Kinetic data for the second step of the photosubstitution of ***[3]***Cl_2 *in* CH_3CN *under* N_2*. a) Globally fitted absorption spectra of the mono-aqua intermediate* $[Ru(dmbpy)(\eta^1\text{-mtmp})(CH_3CN)]^{2+}$ ($[\mathbf{3}\text{-}CH_3CN]^{2+}$*, black) and* $[Ru(dmbpy)_2(CH_3CN)_2]^{2+}$ *(grey) according to modelling using the Glotaran software. b) Modelled evolution of the relative concentrations of* $[\mathbf{3}\text{-}CH_3CN]^{2+}$ *(squares) and* $[Ru(dmbpy)_2(CH_3CN)_2]^{2+}$ *(circles) vs. irradiation time according to global fitting using Glotaran. c) Plot of the amount of* $[\mathbf{3}\text{-}CH_3CN]^{2+}$ *(mol) vs. total amount of photons absorbed by* $[\mathbf{3}\text{-}CH_3CN]^{2+}$ *(mol). The slope of the obtained line is the opposite of the quantum yield of the formation of the bis-aqua complex. Conditions: 0.088 mM solution of* ***[3]***Cl_2 *in* CH_3CN *irradiated at 298 K under* N_2 *using a 521 nm LED at* $6.25 \cdot 10^{-8}$ $mol \cdot s^{-1}$.

AVII.3 Cell growth curves

The growth curves of the two cancer cells under normoxia (21%) or hypoxia (1% O_2) were investigated by seeding the cells at t = 0 and incubating them in the dark. Cells were fixed using TCA at 4, 24, 48, 72, and 96 h after seeding, and then stained with SRB in a cell viability assay. Two biological replicates (nb = 2) were performed to

discard any different impact of the hypoxia depending on the passage number. As shown in Figure AVII.5, under normoxia the two cell lines showed a characteristic exponential growth, with doubling times between 20 and 40 h during the first 72h (Figure AVII.5c). Under hypoxia PC3pro4 cells showed an exponential growth and A549 cells show a less acute exponential growth than under normoxia, with doubling times closer to 40 h. Further incubation to 96 h show differences in the growth depending on the cell line. As shown in Figure AVII.5, cells under normoxia grew faster in the last 24 h of the protocol, whereas under hypoxia this growth stabilized, leading to lower cell confluences.

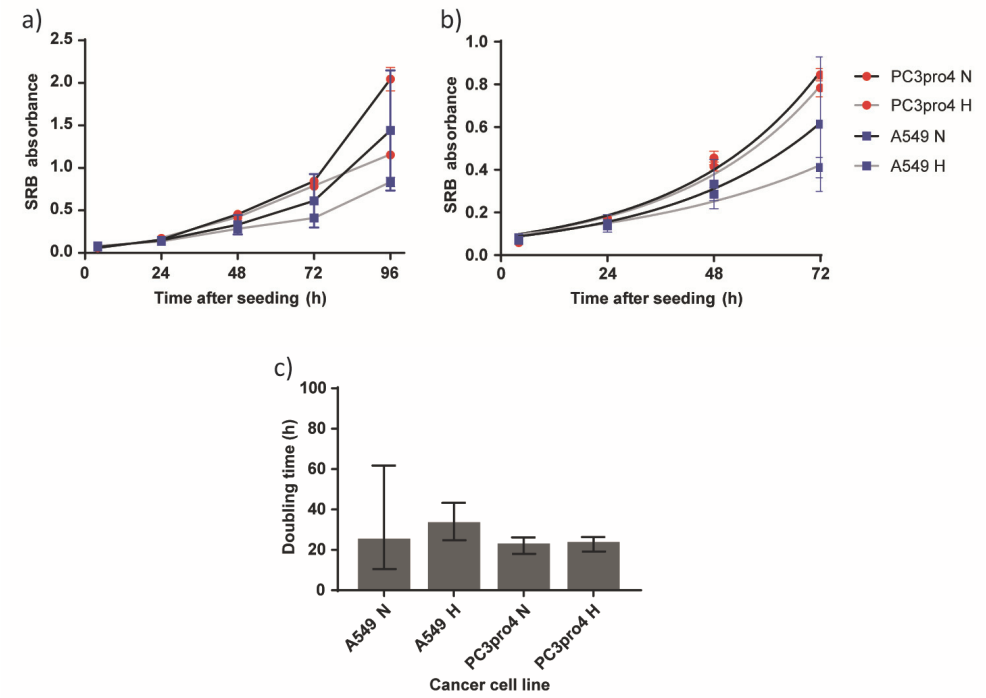

Figure AVII.5. Growth curve (a), fitted exponential growth curves (b), and doubling times with 95% confidence interval (c) for A549 (blue squares) and PC3pro4 (red circles) cancer cell lines under normoxia (N, black line) and hypoxia (H, grey line). Conditions: cells were seeded at time 0 in a 96-well plate using OptiMEM complete and incubetade at 37 °C and either 21% O_2 (normoxia) or 1% O_2 (hypoxia) (A549 N = 5.000 cells/well, A549 H = 6.000 cells/well, PC3pro4 N = 4.000 cells/well, and PC3pro4 H = 4.000 cells/well). Cells were fixed using TCA at 4, 24, 48, 72, and 96 h after seeding and then stained with SRB. The SRB absorbance of ten technical replicates (nt = 10) was averaged for one experiment; two biological replicates were performed (nb = 2).